A Lagrangian Analysis of the Dynamical and Thermodynamic Drivers of Greenland Melt Events during 1979–2017

Reply to both reviewers by Mauro Hermann, Lukas Papritz, and Heini Wernli

We highly appreciate the fruitful and detailed comments of both reviewers, which greatly support investigating the link of atmospheric dynamics and Greenland Ice Sheet (GrIS) surface melt. The greatest concern of both reviewers was the ability of ERA-Interim (1° horizontal resolution) to represent the narrow GrIS ablation zone (20-100 km wide), where the majority of GrIS surface melt occurs. The reviewers highlighted that with "Greenland melt events", as defined in our methods section, we refer to a special category of melt events, i.e., to large-scale melt events affecting the high elevation accumulation zone of the ice sheet. Also, the conclusions drawn from our results on (cloud) radiative effects are only valid for large-scale melt events over the accumulation zone and are not representative of the processes causing melt in the ablation zone. We fully share this view and are grateful for this important critique. The revised version now carefully explains the distinction between ablation zone melt processes and the high-elevation, large-scale melt events, and emphasizes that our study only considers the second type of melt events.

In the following, we group reviewer comments regarding this main concern, and answer them and the remaining comments separately. This document is further supplemented with a latexdiff-pdf (in the same format as the first version of the manuscript) that highlights the modifications made by point-by-point tracking, and to which we will refer in the answers below whenever a specific line number is indicated. Later in the resubmission procedure, we will also submit this revised version of the manuscript.

Reviewer comments 1 by Xavier Fettweis (XF) and 2 by Stefan Hofer (SH) on main concern:

SH: *Scientific assessment:* While the general presentation of the study is to be applauded, there are some distinct methodological limitations that render this study likely to be only valid for a subset of the Greenland Ice Sheet due to the inability to resolve the ablation zone with the ERA-Interim data (i.e. the accumulation zone), and only for a specific type of widespread, long-lasting (24h+) melt events, that also affect the bright interior of the Greenland Ice Sheet, where melt dynamics are significantly different to the ablation zone.
However, as it currently stands the authors draw conclusions on the contribution of clouds, humidity and airmass advection to the general Greenland Ice Sheet melt, which simply cannot be resolved spatially (~100 km resolution). Due to the temporal and elevation focus on widespread melt events, which in themselves can only be driven by large-scale anomalous advection of warm and humid airmasses, it seems that the generalization of the results is likely limited. Overall, more than 80% of all ice melt occurs in the ablation zone - where weather station data shows absorbed shortwave radiation to be the main driver of melt - which is unfortunately not resolved by ERA Interim data in this study.
Because the data used doesn't resolve the darker ablation zone, and the initial selection of melt events likely greatly skews the analysis towards longwave and humidity driven melt events at high elevations, the presented results in their current form cannot be presented as being generally valid to all Greenland melt and likely needs a more nuanced presentation throughout the manuscript.
However, I hope that my comments will encourage the authors to slightly rethink some conclusions of their manuscript, after which this paper will be a welcomed contribution to the growing set of novel Greenland Ice Sheet climate literature.

Authors: Thank you, this comment is extremely helpful, as are the specific comments following below. We fully agree that the findings of our study do not apply to the typical melt in the ablation zone. Instead our study focuses on exceptional, large-scale melt events that affect, in particular, also the elevated accumulation zone, such as during the melt event in summer 2012. In the revised manuscript, we better explain the melt event selection, and the limitations of ERA-Interim to resolve the ablation zone and, therefore, the dominant melt forcing as follows:

1. We refer to the events defined according to our methodology as "large-scale melt events" or "melt events" instead of "Greenland melt events", referring to the terms introduced in the methods (Sect. 2.2). In the title, we replace "Greenland melt events" with "large-scale Greenland melt events". This accounts for the nature and definition of the melt events, as we expect a "large-scale" melt event to fulfill our extent- and elevation-based criteria. We will not highlight the duration of 24h+ in this terminology due to the procedure of connecting melt time steps, which are separated by up to 24h.
2. When introducing the trajectory setup (Sect. 2.3., L148), we highlight that the vast majority of the starting points lies in the accumulation zone, shown by the percentage of starting points above 1000/1500/2000m (90%/76%/56%).
3. We introduce our research questions more clearly (especially in L91-93), such that it becomes clear that we focus on – and thus, the answers to the research questions are valid for – large-scale melt events including the accumulation zone.
4. ERA-Interim resolution: Our intention is to resolve the large-scale atmospheric flow prior to the defined melt events, and to understand how this then affects the GrIS surface conditions in different regions (S, W, N, E, C instead of ablation/accumulation zone). We fully agree that the ablation area is not at all resolved in ERA-Interim, and our conclusions should only concern either the trajectory history prior to melt events or accumulation zone radiative effects. However, these melt events mostly cover large parts of the ablation area as well, which is why it would not be entirely correct to only refer to the accumulation zone. Of course, when specifically looking into cloud and moisture radiative effects, our analysis cannot attribute a cause of melt to ice in the ablation area (see below). But the ablation area is affected by the synoptic situation described in our study as well. Thus, we tried to better balance the fine line of framing our conclusions correctly. They should clearly not attribute a cause to ablation area melt, but they should neither exclude the effect of the atmospheric circulation on the entire GrIS during large-scale melt events.

SH: *Title*: Maybe include "of large-scale" or "extreme" melt events, because for the reader it seems that the authors focus primarily on a very specific subset of melt events, that might not represent the general physical mode of "normal" melt.

Authors: Thank you for this suggestion, which we like very much. We changed the title to "A Lagrangian Analysis of the Dynamical and Thermodynamic Drivers of *Large-Scale* Greenland Melt Events during 1979–2017". While the melt events selected in our study are certainly exceptional, we prefer, however, not to include "extreme" in the title given that we find 77 melt events in less than 40 years.

SH: *Introduction*: The introduction was very enjoyable to read and is a very concise account of the current state of the relevant Greenland literature. Around L90 – the main questions the authors want to answer. Q1) "How often did melt events occur over the GrIS during 1979-2017?" Maybe mention that the authors focus on widespread, long-lasting melt events that affect the bright ablation zone. Q3) Also potentially highlight that the radiative effects and air mass modifications are valid for your chosen subset of melt events, not the "normal" GrIS melt. Q4) "Does the answer to Q2 and Q3 differ for subregions of the GrIS?" → For the reader the most interesting question would likely be does it differ for the accumulation zone melt events vs. the ablation zone melt events where more than 80% of all melt occurs and where the physical drivers are significantly different due to the difference in albedo.

Authors: We agree with your suggestions. We reword our main research questions (L100-104) to:

- Q1) How often did *large-scale* melt events occur over the GrIS during 1979–2017?
- Q2) What are the synoptic flow configuration and the air mass pathways during *these* melt events?
- Q3) Which thermodynamic air mass modifications and radiative effects *over the GrIS accumulation zone* caused these melt events?
- Q4) Does the answer to Q2 and Q3 differ for subregions of the GrIS *accumulation zone*?

We now discuss the difference of our melt event results (longwave radiative forcing) and the typical shortwave-dominated ablation zone melt in the discussion section (L579 onwards) based on the results of known literature (Hofer et al., 2017, Wang et al., 2019, Izeboud et al., 2020). In addition, we address ablation area melt separately in the introduction (L50-65).

SH: L94 ff – Era Interim data: At 1° resolution the ERA Interim data does give the authors one pixel in the SW of the GrIS where the ablation zone is at its widest and even less where the ablation zone lies in steeper terrain. Both is not sufficient to resolve the ablation zone. For the reader it seems that the study design is robust to answer Q2 mentioned in the introduction, but Q1, Q3 and Q4 can only be answered for the accumulation zone.

Authors: Absolutely correct, see previous comments.

SH: L111 For the reader it likely needs to be made clearer throughout the manuscript that the authors are dealing with a specific subset of widespread melt events, and not the ablation zone melt dynamics that contribute most to GrIS melt.

Authors: We now highlight our focus on *large-scale* melt events in the title and abstract, instead of using the too generic term "Greenland melt events". The introduction more clearly differentiates between radiative processes affecting the ablation vs. the accumulation zone and better emphasizes the focus of our study (see above). Furthermore, we emphasize our melt event definition in the method section (L118, L120, L129, L148) and remind the reader in the result subsections (L311, L342-345, L371, L455).

SH: L319 "In this section we generalize the results from the EV69 case study by considering all 77 Greenland melt events." I think this statement is somewhat misleading. The authors are not generalizing to "all" melt events, but still only to a subset of widespread and longwave driven melt events that reach up to high elevations and last longer than 24h. For the reader this nuance is lacking through most parts of the following and preceding discussion of results and should be added throughout, also that ERA I does not resolve the ablation zone.

Authors: Already in the previous form of the manuscript, we chose a specific terminology "Greenland melt events" referring to events as defined in the method section, and carefully made use of this terminology throughout the manuscript. We acknowledge the nuance mentioned here, and will carefully define the term "melt events" in the methods section to avoid confusion with statements about general "Greenland melt events". Also, we change the terminology in the specific sentence to "all 77 large-scale melt events" (L342). We prefer this terminology over somewhat lengthy terms such as "large-scale melt events affecting the GrIS accumulation zone" which would make the manuscript quite cumbersome to read.

Regarding the comment on ERA-Interim resolution, we completely agree (see answer to the first remaining comment by XF below).

SH: L374 "… but now for all Greenland melt events in JJA 1979-2017" See previous comment on why this might be an overstatement.

Authors: Agree, see above. Changed to "for all 77 large-scale melt events in JJA 1979-2017" in L371.

XF: When the impact on the net surface solar radiation is discussed (eg: Figs 7 and 13), the presented results are depend of the ERA-Int resolution (100km) which is not enough to represent the ablation zone (with a lot of lower surface albedo than snow and a width typically lower than 100km). Moreover, I'm not sure that ERA-Int is able to represent the bare ice albedo (0.3-0.5) when the ablation zone is larger than 100km. Therefore, this issue should be absolutely discussed in the manuscript and the conclusions discussed in Section 4.3 (lines 452-465) are in fact only valid in the accumulation zone as the ablation zone is not really represented here by ERA-Interim. In the ablation zone, as discussed in Hofer et al. (2017), the shortwave anomalies drive the melt and clouds have a cooling effect.

SH: L426 and following section "Linkage to clouds and radiative effects" The authors likely need to take into account the limitations of their approach here. The used data simply doesn't allow to answer the question of what is driving most of the GrIS melt, given that a great majority of melt occurs in the ablation zone that isn't resolved here. Additionally, the chosen subset of melt events skews the conclusion drawn for the contribution of radiation and clouds to quite obviously longwave driven melt events in the bright accumulation zone of the Greenland Ice Sheet. For the reader this section needs quite a bit more of a nuanced assessment, especially from L448 onwards, where the authors conclude that the longwave radiative effect of clouds and humidity is the main contributor to melt and enhanced furthers by anticyclonic circulation.

Authors: Both comments highlight the need for a short discussion of the limitations of our approach. We now outline in the introduction (L77, L91-93) and method section (see above) that our focus lies on (i) the large-scale air mass transport and modifications before large-scale melt events, and (ii) on exceptional, large-scale melt events affecting the high-albedo/elevation accumulation zone.

Then, most importantly, the conclusions drawn in Sect. 4.3 were strongly reduced, such that it becomes clear to the reader that our main focus lies on the subsections before (air mass modifications during large-scale melt events). The main result drawn from Sect. 4.3, namely that these air masses enhance longwave radiative forcing as known for the GrIS accumulation zone, is highlighted more accurately (L474-499).

Furthermore, we will discuss the limitations of ERA-Interim (horizontal resolution, boundary layer representation) in the discussion and conclusion section (see first remaining comment by XF).

SH: L523 ff "longwave radiation is a key element in triggering surface melt in Greenland and the remaining Arctic". The results here are only representative for the accumulation zone melt dynamics and not Greenland in general. Unfortunately, this statement cannot be concluded from the presented analysis.

Authors: Yes → changed to "in the GrIS accumulation zone and the remaining Arctic" in L572.

SH: L528 ad "ii) causing a positive cloud radiative effect" – Yes, but this can only be answered here for the interior of the GrIS where the surface albedo is high and therefore the cloud radiative dynamics are significantly different to the ablation zone (additional to a skewed subset of melt events). Just today a paper has been published that shows that the CRE is negative over the GrIS ablation zone during summer, and positive over the accumulation zone. (https://agupubs.onlinelibrary.wiley.com/doi/epdf/10.1029/2020GL087315).

Authors: Thank you, this study is very useful for discussing the cloud radiative effects and especially for differentiating between ablation and accumulation zone melt. We include it to put our results of accumulation zone melt into perspective (L499, L580, L584).

XF: The results presented here are based on ERA-Interim. I don't ask to redo this study using the new generation ERA5 reanalysis, but the use of ERA5, improving a bit the representation of the near surface condition over the ice sheet (Delhasse et al., 2020) and available at a higher resolution (30km) more suitable to represent the ablation zone, could be also mentioned in the perspective.

Authors: We now provide an outlook in the discussion and conclusion section that addresses this issue (L579-589), including a reference to Delhasse et al. (2020). There, we mention the limitations of ERA-Interim, and refer to ERA5 and/or regional climate models (MAR, RACMO), which are better suited for studying local melt processes, for comparison to in situ measurements, and for surface energy fluxes thanks to their higher resolution of the steep topography and improved albedo.

Remaining comments by XF (RC1):

This paper discusses the origin of air masses generating melt events over the ice sheet by focusing first on July 2012 as example and after to the 1979-2017 climatological mean. While this paper is quite complex (high scientific level) and not easy to understand after a quick first reading, it is very original, with a clear aim and certainly deserves to be accepted for publication. I have however several (minor) remarks:

- When the authors are discussing the origin of air masses, it is not clear which vertical level is considered? A height of 20, 40, 60 hPa above the Greenland ice sheet surface is mentioned. Which one is used? How are the authors sure that the considered level is not in the boundary layer and then, impacted by the katabatic winds for example?

  Authors: We average these three layers in our analyses (LFP maps, e.g., Fig. 3) to account for potential deficiencies of ERA-Interim in representing the boundary layer over the GrIS. In our study we are interested in the origin, transport pathways, and modifications of air masses present near the surface during large-scale melt events (highlighted now in L152). Choosing 20, 40, and 60 hPa above the surface as starting positions allows us to select air masses in the proximity of the surface, while at the same time avoiding potential deficiencies of ERA-Interim in representing the detailed structure of the boundary layer above the GrIS [a highly important layer for surface melt, e.g., Ohmura et al. (2001)]. Furthermore, we assume the representation of the near-surface flow in ERA-Interim to be sufficient for our study design, as we focus on air mass modifications on a time-scale of ten days and air mass movement of several thousand kilometers.

  Still, we fully agree that it is important to include a discussion of the resolution and limitations of ERA-Interim in the discussion and conclusion section (L579-589). Our intention is not to resolve the detailed processes in the ablation zone, nor to make use of the (insufficient) abilities of ERA-Interim to represent boundary layer processes such as katabatic drainage flows. We therefore clearly point out that we focus on the large-scale atmospheric transport/modification of air masses arriving close to the GrIS surface during large-scale melt events, i.e., over the accumulation zone (see above). Our set of melt events could be the starting point for studies of the detailed boundary layer processes during these events using RCM or in situ data.

- While Summer 2019 is not studied here, I would like to mention that the 01-AUG-2019 big melt event was generated by air masses coming from Europe and having crossed North-Atlantic (Tedesco and Fettweis, 2020). Such an origin in a melt event is not mentioned here suggesting that such origin is very exceptional and such an event deserves to be studied in further studies.

Authors: This is an interesting point. We supplement our manuscript with a figure showing the trajectory density of all 77 large-scale melt events together, at different times before arrival over melting parts of the GrIS during a melt event (see below, based on the gridding tool v2.4.2; Škerlak, 2014). There are two tongues of increased trajectory density stretching over Scandinavia and Great Britain. From the cyclonic movement of the tongue between t=–192h and t=–96h (Figs. S2a-c), it seems likely that some of the melt events show a similar air mass origin and transport pathway as the 1 August 2019 event, likely linked to a cyclone near Great Britain and an anticyclone over (West) Greenland. Nevertheless, the bulk of the air masses clearly originates from west of Greenland, indicating that transport pathways as during the 1 August 2019 event are rather exceptional, which we focus on in L379-383.

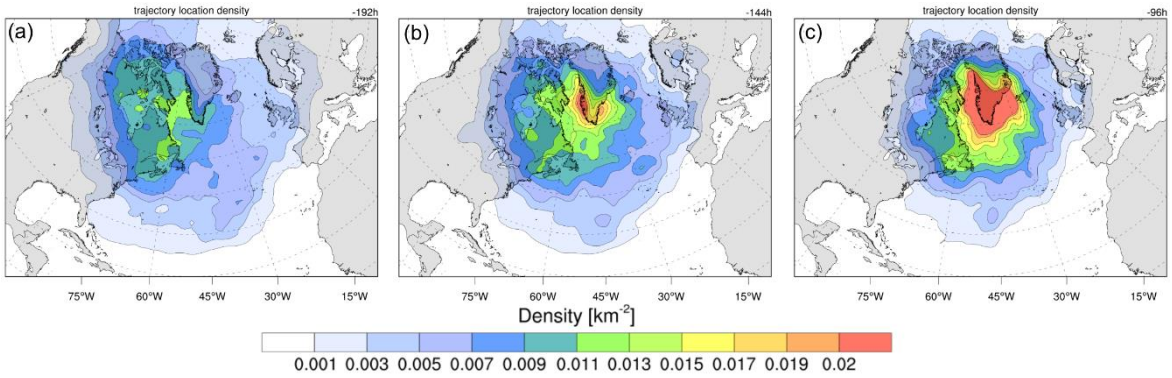

Remaining comments by SH (RC2):

In this study, Hermann et al. present a Lagrangian analysis of one specific melt event in summer 2012 and 77 long-lasting melt events between 1979-2017. The authors use a threshold value for the surface temperature of -1°C to identify melt from the ERA Interim dataset. The authors focus on more extreme, widespread melt events with more than 5% of Greenland melting simultaneously, melt occurring above 2000m and only focus on melt events lasting for more than 24 hours. Additionally, the authors also use ERA Interim data to try and establish the underlying drivers of melt events (surface radiative fluxes, liquid water content and others). Furthermore, the authors establish a novel way to identify the main areas of synoptic-scale airmass advection prior and during these 77 more pronounced melt events.
Overall, this study is very well written and consists of a set of nicely presented figures. The approach the authors use is scientifically novel and has the potential to shed some light on the question of how circulation and advection patterns influence Greenland melt.

Specific comments by SH:

L135 Is there a previous study that looks at the capabilities of ERA-Interim to accurately model the GrIS boundary layer, given that all the parcels of the authors are starting in the lowermost 500m of the atmosphere?

Authors: We are not aware of a study that systematically evaluated the boundary layer over the GrIS in general. However, several studies investigated the representation of specific parameters such as near surface winds, surface temperature, or long- and shortwave radiative fluxes in the Arctic in general and over the GrIS in particular against in situ observations. These studies agree that among state-of-the-art reanalyses, ERA-Interim performs particularly well (Chen et al. 2011, Cox et al. 2014, Lindsay et al. 2014, Wesslén et al. 2014, Fettweis et al. 2017). Furthermore, Delhasse et al. (2020) found certain improvements of ERA5 compared to ERA-Interim over the GrIS in terms of surface variables such as 2m temperature or 10m winds, but noted that the differences are not significant.

For the purpose of our study, it is especially important that the large-scale wind fields are properly represented such as to capture the air mass transport onto the GrIS appropriately. Moore et al. (2013) and Oltmanns et al. (2014) compared wind fields with station data and found generally a good agreement over Greenland, emphasizing in particular also the capability of ERA-Interim to represent downslope windstorms. However, Moore et al. (2013) also noted that – common to coarse resolution models – turbulence parameterizations are too diffusive, leading to too deep boundary layers and too weak temperature inversions.

By starting trajectories not just from the surface but instead from 20, 40, and 60 hPa agl, we capture the bulk of near-surface air masses arriving over the GrIS. This is appropriate for our study focusing on the large-scale spatial and temporal evolution (10 days, thousands of kilometers) of the air masses arriving over the GrIS.

L195 How did the authors identify the "dry intrusion" near Newfoundland? Isentropic potential vorticity based analysis?

Authors: We did not define this airstream as dry intrusion → Changed "descended in the dry intrusion" to "descended cyclonically in the low near Newfoundland" in L212.

L270 ff Discussion about previously warm and humid airmasses losing their warm anomaly but staying humid. Might it potentially not be better to look at a variable that combines temperature and humidity, such as equivalent potential temperature, to define an airmass? Is there a specific reason why the authors chose not to?

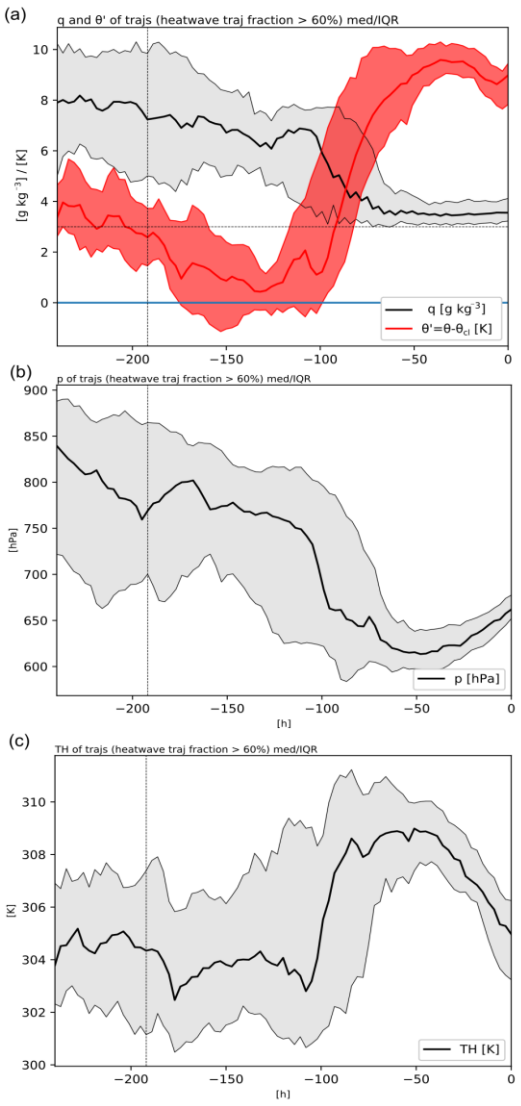

Authors: This paragraph should shed light on whether the potential temperature anomaly over the U.S. Great Plains was the start of the potential temperature anomaly over Greenland. Equivalent potential temperature would indeed be useful as a tracer for humid air masses, but it would obscure warming by condensation of water vapor, which appears important for the formation of the final temperature anomaly. We use the LAGRANTO trajectory tool to trace the air mass, and then look into why it became anomalously warm (it is important to note that THanom indicates the potential temperature anomaly of the air mass wrt. the local climatology.

The figure added here additionally illustrates the potential temperature and pressure evolution along the heat wave trajectories. We can conclude that the strong increase in THanom by almost 10K between t=–120h and t=–48h can be attributed to: (i) Net 6K diabatic heating (panel c) due to latent heat release during ascent of ~150hPa and overcompensated radiative cooling (panel b), (ii) transport into a climatologically 4K colder region (of course Greenland is more than 4K colder than the U.S. East coast, but the air masses also ascend to higher altitudes). The amount of diabatic heating fits to the 6K diabatic heating of C air masses apparent from the TH-T diagram (Fig. 12c).

L284 “cloud formation” Until this point the authors did not look at clouds specifically, so some of the changes in radiative fluxes could be due to phase change in existing clouds alone and not just due to extra cloud formation.

Authors: Good point, changed “cloud formation and latent heating” → “latent heating from condensation of water vapor” (L303).

L289 How robust is the phase partitioning in the atmospheric column, i.e. is the total column liquid water in ERA-I reliable in high-latitudes? Maybe there is a study to cite that looks at this specifically.

Authors: Overall, ERA-Interim represents the liquid water path in the Arctic relatively well and at times better than models with a more complex microphysics scheme (cf. Wesslén et al. 2014) – now mentioned in L313. However, there are certain known biases especially over the GrIS. For instance, Bennartz et al. (2013) found that in summer ERA-Interim underestimates the occurrence of thin liquid clouds at Summit.

L295 Interestingly, it seems that in the NW of the GrIS there is even a negative anomaly of liquid water content in lower elevation areas, and only when the airmass ascents further it suddenly develops a positive liquid water content anomaly. Any ideas of why that is, given that the airmass in itself likely has a higher specific humidity content than in the climatology overall?

Authors: This is indeed an interesting phenomenon, as the NW region showed melt to high elevations during most of EV69. However, lower elevations were approached by normal to slightly colder air masses in the beginning of EV69 (see Fig. 1b). There are two air streams at play: N1 representing the air stream arriving at higher elevations (warm-moist) and N2 being somewhat representative of air masses reaching the lower elevations from the Northwest (and also Northeast; Fig. 2). N1 trajectories reach saturation in the very end, and the further they ascend, the further they carry liquid cloud water, the positive TCLW anomaly, and the negative SSRD anomaly inland. Conditions over the lower NW region are mostly sunnier than climatology, i.e., clouds are thinner or still contain ice at higher altitudes (the SSRD’ median is positive in this region (Fig. 7g shows the average)). The transition of negative to positive TCLW’ thus represents the interaction/boarder of the two air streams.

L295-308 Maybe the authors could mention that the discussion here is still focusing at one specific melt event? Sometimes this wasn’t clear for the reader.

Authors: We will add in the introducing sentence of this paragraph “during EV69” in L317.

References:

Chen, L., Johannessen, O., Wang, H., and Ohmura, A.: Accumulation over the Greenland Ice Sheet as Represented in Reanalysis Data, Adv. Atmos. Sci., 28, 1030–1038, https://doi.org/10.1007/s00376-010-0150-9, 2011.

Cox, C. J., Walden, V. P., Compo, G. P., Rowe, P. M., Shupe, M. D., and Steffen, K.: Downwelling longwave flux over Summit, Greenland, 2010–2012: Analysis of surface-based observations and evaluation of ERA-Interim using wavelets, J. Geophys. Res.-Atmos., 119, 12317–12337, https://doi.org/10.1002/2014JD021975, 2014.

Fettweis, X., Box, J. E., Agosta, C., Amory, C., Kittel, C., Lang, C., van As, D., Machguth, H., and Gallée, H.: Reconstructions of the 1900–2015 Greenland ice sheet surface mass balance using the regional climate MAR model, The Cryosphere, 11, 1015–1033, https://doi.org/10.5194/tc-11-1015-2017, 2017.

Hofer, S., Tedstone, A. J., Fettweis, X., and Bamber, J. L.: Decreasing cloud cover drives the recent mass loss on the Greenland ice sheet, Sci. Adv., 3, e1700 584, https://doi.org/10.1126/sciadv.1700584, 2017.

Moore, G. W. K., Renfrew, I. A., and Cassano, J. J.: Greenland plateau jets, Tellus A: Dynamic Meteorology and Oceanography, 65:1, https://doi.org/10.3402/tellusa.v65i0.17468, 2013.

Oltmanns, M., F. Straneo, G. W. K. Moore, and Mernild, S. H.: Strong downslope wind events in Ammassalik, southeast Greenland. J. Climate, 27, 977–993, https://doi.org/10.1175/JCLI-D-13-00067.1, 2014.

Škerlak, B.: Climatology and process studies of tropopause folds, cross-tropopause exchange, and transport into the boundary layer. PhD thesis, ETH Zurich. https://doi.org/10.3929/ethz-a-010256937, 2014.

Wang, W., Zender, C. S., van As, D., and Miller, N. B.: Spatial distribution of melt season cloud radiative effects over Greenland: evaluating satellite observations, reanalyses, and model simulations against in situ measurements, J. Geophys. Res. Atmos., 124, 57–71, https://doi.org/10.1029/2018JD028919, 2019.

Wesslén, C., Tjernström, M., Bromwich, D. H., de Boer, G., Ekman, A. M. L., Bai, L.-S., and Wang, S.-H.: The Arctic summer atmosphere: an evaluation of reanalyses using ASCOS data, Atmos. Chem. Phys., 14, 2605–2624, https://doi.org/10.5194/acp-14-2605-2014, 2014.

A Lagrangian ~~Analysis~~ analysis of the ~~Dynamical~~ dynamical and ~~Thermodynamic Drivers~~ thermodynamic drivers of large-scale Greenland ~~Melt Events~~ melt events during 1979–2017

Mauro Hermann[1], Lukas Papritz[1], and Heini Wernli[1]

[1]Institute for Atmospheric and Climate Science, ETH Zürich, Zurich, Switzerland

Correspondence: Mauro Hermann (mauro.hermann@env.ethz.ch)

Abstract.

In this study, we systematically investigate the dynamical and thermodynamic processes that lead to 77 ~~Greenland~~ large-scale melt events affecting high-elevated regions of the Greenland Ice Sheet (GrIS) in June–August (JJA) 1979–2017. For that purpose, we compute 8-day kinematic backward trajectories from the lowermost ∼500 m above the GrIS during these events. The key synoptic feature accompanying the melt events is an upper-tropospheric ridge southeast of the GrIS associated with a surface high pressure system. This circulation pattern is favourable to induce rapid poleward transport (up to 40° latitude) of warm (∼15 K warmer than climatological air masses arriving on the GrIS) and moist air masses from the lower troposphere to the western GrIS and subsequently to distribute them in the anticyclonic flow over North and East Greenland. During transport to the GrIS, the melt event air masses cool by ∼15 K due to ascent and radiation, which keeps them just above the critical threshold to induce melting. The thermodynamic analyses reveal that the final warm anomaly of the air masses is primarily owed to anomalous horizontal transport from a climatologically warm region of origin. However, before being transported to the GrIS, i.e., in their region of origin, these air masses were not anomalously warm. Latent heating from condensation of water vapour, occurring as the airstreams are forced to ascend orographically or dynamically, is of secondary importance. These characteristics were particularly pronounced during the most extensive melt event in early July 2012, where, importantly, the warm anomaly was not preserved from anomalously warm source regions such as North America experiencing a record heat wave. The mechanisms identified here are in contrast to melt events in the low-elevation high Arctic and to midlatitude heat waves, where adiabatic warming by large-scale subsidence is essential. Considering the impact of moisture on the surface energy balance, we find that radiative effects are closely linked to the air mass trajectories and enhance melt over the entire GrIS accumulation zone due to (i) enhanced downward longwave radiation related to poleward moisture transport and a shift in the cloud phase from ice to liquid primarily west of the ice divide, and (ii) increased shortwave radiation in clear-sky regions east of the ice divide. Given the ~~identified mechanisms that cause extensive melt over the GrIS~~ongoing increase of the frequency and the melt extent of large-scale melt events, the understanding of upper-tropospheric ridges over the North Atlantic, i.e., also Greenland blocking, and its representation in climate models is crucial in determining future GrIS accumulation zone melt and so global sea-level rise.

1 Introduction

The Greenland Ice Sheet (GrIS) is the world's second largest ice body holding water equivalent to $6-7$ m of global sea level rise (Ridley et al., 2005). Its mass loss due to surface melt and ice discharge has increased strongly over the past 120 years and equaled $286 \pm 20\,\mathrm{Gt\,yr^{-1}}$ in 2010–2018 (Kjeldsen et al., 2015; Mouginot et al., 2019). Not only the current magnitude, but also the speedup of mass loss from the GrIS, observed recently and predicted for the future, are primarily driven by a negative surface mass balance (Enderlin et al., 2014; Van den Broeke et al., 2016). Surface melt has been increasing in the last decades and appears to be the major regulator of the surface mass balance (Box et al., 2004; Fettweis et al., 2012; Andersen et al., 2015; Van den Broeke et al., 2016). At the same time, snow accumulation has decreased since the early 2000s, due to a reduced frequency of cyclones and increased frequency of anticyclones in the close vicinity of Greenland (Chen et al., 2016). Consequently, both contributors to the surface mass balance have favored a stronger mass loss from the GrIS, with melt as the primary factor.

While GrIS melt is highly sensitive to the atmospheric forcing (Hanna et al., 2005), the oceanic forcing during summer melt events is often weak (e.g., Hanna et al., 2014) and the influence of high sea surface temperatures on the GrIS surface mass balance is generally limited due to the katabatic wind blocking effect (Noël et al., 2014). Two largely anti-correlated indices based on geopotential height are often used to capture the dominant modes of variability of the large-scale circulation in the North Atlantic: the North Atlantic Oscillation (NAO) index (Hurrell et al., 2013) and the Greenland Blocking Index (GBI; Hanna et al., 2013). While the NAO captures the strength of the westerly flow over the North Atlantic, the GBI characterises geopotential height anomalies over Greenland with a positive index representative of anticyclonic flow and at times atmospheric blocking. A series of warm summers (June-August, JJA) since the late 1990s were linked to a doubled anticyclone frequency over Greenland compared to the past 50 years (Fettweis et al., 2013). Such anticyclonic conditions are typical for periods with a negative NAO index and positive GBI (NAO-/GBI+). They are characterized by a northward displaced jet stream over Greenland, which favors anomalous meridional transport. This leads to high temperatures in South and West Greenland, but colder conditions and below-average ice loss in Svalbard (Fettweis et al., 2013; Box et al., 2018).

~~Radiative and turbulent~~ Radiative heat fluxes are ~~both~~ known to contribute substantially to melt ~~events over the GrIS (e.g., Fausto et al., 2016; Hofer et al., 2017). Specifically, Hofer et al. (2017) attributed much of the decrease of the surface mass balance during the past 20 years to the GrIS-wide decrease in optically thick clouds, i.e., additional downward shortwave radiation.~~ over both the GrIS ablation and accumulation zone. While clouds block incident shortwave solar radiation (Hofer et al., 2017), they~~—~~, together with higher water vapour content~~—~~, tend to enhance downwelling longwave radiation (e.g., Ohmura, 2001; Van Tricht et al., 2016; Gallagher et al., 2018). The net cloud radiative effect caused by these opposed influences depends on ~~cloud properties and~~ the surface albedo and cloud properties - especially the thickness and cloud water phase (Hofer et al., 2019) - and thus varies in sign and magnitude over the GrIS ~~(Box et al., 2012; Wang et al., 2019). Hofer et al. (2019) highlighted the relevance of the cloud liquid water phase in determining the sign of the cloud radiative~~

effect . At Summit(Wang et al., 2019; Izeboud et al., 2020). In the low albedo ablation zone, where the majority of surface melt occurs, optically thick clouds have a cooling effect and their reduction in the past 20 years coincided with enhanced surface mass loss (Hofer et al., 2017). Contrarily in the high albedo accumulation zone, clouds were found to have a warming effect due to downward longwave radiation, which was particularly pronounced in summer 2012 (Bennartz et al., 2013; Miller et al., 2015; Van Tricht Furthermore, moist-warm conditions and more importantly liquid clouds are not only instantaneous drivers of melt, but their effect also accumulates over time to precondition surface melt, on daily (Solomon et al., 2017), seasonal (Park et al., 2015) and annual time scales (Tedesco et al., 2013).

The transport of anomalously warm and humid air masses is a key driver of individual large-scale melt events over the GrIS. Warm Warm-moist air implies strong sensible heat non-radiative energy fluxes into the ice, such as for example in July 2012 (Hanna et al., 2014; Fausto et al., 2016). During that period, the transport of warm air from a concurrent heat wave over North America (Hoerling et al., 2014) to the GrIS was suggested to be directly related to two melt events peaking at 98% and 79% melt extent (Neff et al., 2014). Additionally, the involved moisture transport from the western subtropical North Atlantic triggered cloud radiative effects favorable for melt of the GrIS surface melt in the accumulation zone (Neff et al., 2014; Bonne et al., 2015). Optically thin liquid clouds increased the downward longwave radiative fluxenhanced downward longwave radiation, still letting shortwave radiation penetrate, and enabled surface melt over the normally dry GrIS inland plateau (Bennartz et al., 2013). In addition to the aforementioned effectsAdditionally, air temperature near the surface directly affects the downwelling longwave radiative fluxes since the bulk of these is emitted in the lowermost kilometer of the atmosphere (Ohmura, 2001). Hence, in this study As such large-scale melt events are expected to become more frequent, we will focus on the mechanisms that lead to the presence of anomalously warm air masses over the GrIS air masses arriving during such periods near the GrIS surface.

Three processes can, in principle, contribute towards the formation of a warm temperature anomaly of airstreams reaching the GrIS (Papritz, 2020), namely the transport of an already warm air mass from a climatologically warmer region towards the GrIS, adiabatic compression during subsidence, and heating by diabatic processes. The latter comprises radiation, latent heat release in clouds, and turbulent surface fluxes (e.g., Holton and Hakim, 2012). In particular, subsidence is known to be an essential contributor to mid-latitude heat waves (Bieli et al., 2015; Zschenderlein et al., 2019) and warm anomalies in the high Arctic (Ding et al., 2017; Wernli and Papritz, 2018; Papritz, 2020). Furthermore, turbulent surface fluxes over the ocean are typically limited in summer due to the small surface-atmosphere temperature gradient.

Given the high importance Considering the relevance of the atmospheric circulation for the variability of Greenland's near-surface temperatureclimate, the goal of our study is to improve our understanding of the atmospheric dynamical processes leading to extensive melt episodes over the GrIS melt episodes that cover large parts of the GrIS accumulation zone. This knowledge is also relevant given the important given the strong impact of such exceptional melt events on the surface mass balance and the expected increase of GrIS mass lossand the ice sheet's melt extent, mass loss, and contribution to global sea

level rise~~, and~~. Furthermore, it might shed light on climate models struggling to simulate the observed circulation anomalies (e.g., Fettweis et al., 2012, 2013). More precisely, this study has two main objectives: First, we want to go beyond case studies and investigate large-scale melt events systematically in the period of 1979–2017. Still, the well-studied and most ~~extreme~~ extensive melt event of July 2012 will serve as an excellent example to illustrate our methods and findings. Second, we aim to investigate the history and thermodynamic evolution of air masses associated with ~~Greenland~~ large-scale melt events with the aid of Lagrangian backward trajectories. This approach will enable us to answer the following questions:

Q1) How often did large-scale melt events occur over the GrIS during 1979–2017?

Q2) What are the synoptic flow configuration and the air mass pathways during these melt events?

Q3) Which thermodynamic air mass modifications and radiative effects over the GrIS accumulation zone caused these melt events?

Q4) Does the answer to Q2 and Q3 differ for subregions of the GrIS accumulation zone?

2 Data and ~~Methods~~methods

2.1 ERA-Interim data

This study is based on ERA-Interim reanalysis data from the European Centre for Medium-Range Weather Forecasts (ECMWF; Dee et al., 2011). The data is available every 6 h from 1979 to 2017, on 60 vertical levels and interpolated to a grid with a horizontal grid spacing of 1°. The reanalysis data serves as best estimate of the past atmospheric state on the synoptic scale, which is why we implicitly refer to it as the actual state of the atmosphere. As climatologies of the variables used for Eulerian analyses (Table 1), we compute 10 d-averages of the 6-hourly data centered on the respective calendar day over the entire period 1979–2017~~(i. e., the long-term average of 39 x 41 time steps).~~. Note that for radiation, we use fields with the same time of day only to account for the daily cycle~~(i. e., 39 x 11 time steps).~~. We use the ice outline after Zwally et al. (2012) to separate ice from land grid cells in Greenland. Only grid cells with a center inside the ice outline are classified as ice grid cells, which leads to ~~519 ice grid points in ERA-Interim, corresponding to~~ a GrIS area of 1.73 million km^2, which is slightly larger (+0.7%) than observed (Zwally et al., 2012).

2.2 Melt event definition

As previous studies focused on single ~~Greenland~~ large-scale melt events, such as in July 2012 (e.g., Nghiem et al., 2012; Bennartz et al., 2013; Tedesco et al., 2013; Neff et al., 2014; Bonne et al., 2015), there is yet no generally accepted definition of ~~a melt event~~ such melt events for climatological studies. We define them as follows: The occurrence of surface melt is approximated by a skin temperature (*SKT*) greater or equal to −1°C, as in earlier studies (e.g., Nghiem et al., 2012). A time step is interpreted as part of a melt event if at least 5% of the total GrIS surface area is melting and ~~including grid points~~ located above 2000 m elevation (“melt time step”), to distinguish melt events from the typical summer melt in the GrIS ablation area. In order

to avoid splitting of a - from a dynamical point of view - coherent melt event due to the pronounced diurnal temperature cycle, we include non-melt time steps when identifying coherent melt events. This is done as follows: intermediate non-melt and melt time steps are connected in time to yield melt events with the starting (end) date defined as the first (last) time step when melt was detected, but not preceded (followed) by melt for more than 24 hours. The thresholds of 5% and 2000 m were chosen with hindsight, such that a reasonable maximum melt event duration of around two weeks and a sufficiently large sample size of 77 melt events results. Events shorter than 24 hours are neglected. To summarize, we focus on melt events that cover a wide area of the GrIS accumulation zone and hereafter refer to them as "large-scale melt events" or "melt events" for simplicity.

The 77 ~~Greenland~~ melt events in 1979–2017 (Tables S1–S3) lasted between 1.25 d and 16.25 d and on average 4.1 ± 3.4 d (Table 2). Surface melt during short events typically covered around a third of the GrIS at maximum. On average, about half $(44.6 \pm 10.7\%)$ of the GrIS was melting at the time of maximum extension of the event. The three melt events affecting the largest ice area were EV69 (94.8%), EV35 (83.9%) and EV70 (70.3%) in early July 2012, June 2002 and end of July 2012, respectively. EV69 is the most closely investigated melt event in the literature, where surface melt occurred up to the highest ERA-Interim grid point at 3175 m. Considering all events, the maximum elevation with surface melt was 2692 ± 193 m. The maximum two-meter temperature at the most elevated grid point experiencing melt averaged slightly below 0°C.

2.3 ~~Trajectories~~Backward trajectories

~~In addition to the classical way of depicting atmospheric phenomena from the Eulerian perspective, we~~ We use the Lagrangian framework to investigate air mass modifications, the underlying physical processes and general flow structures. The Lagrangian analysis tool LAGRANTO (Wernli and Davies, 1997; Sprenger and Wernli, 2015) basically solves the trajectory equation

Table 1. The ERA-Interim variables used for the evaluation of the synoptic situation over the GrIS ("Eulerian variables").

Eulerian variables		
abbreviation	**variable name**	**unit**
RR	6 h-accumulated rainfall	[mm]
SF	6 h-accumulated snowfall	[mm]
SSR(D)	(downward) surface shortwave radiation	[W m^{-2}]
STR(D)	(downward) surface thermal radiation	[W m^{-2}]
TCVHT	total column horizontal water vapour transport	[kg m^{-1} s^{-1}]
TCV	total column water vapour	[kg m^{-2}]
TCIW/TCLW	total column ice/liquid water	[kg m^{-2}]
Z500	500 hPa geopotential height	[m]
$\theta_{10\mathrm{m}}$	potential temperature on the lowest model layer ($\sim$10 m)	[K]

Table 2. Average (Avg.), standard deviation (σ), minimum (Min.) and maximum (Max.) of melt event duration, maximum elevation experiencing surface melt (ME) and maximum two-meter temperature (*T2M*) at this highest grid point, respectively, as well as minimum and maximum melt extent during the melt event. For *T2M@ME*, the elevation at which it was observed is indicated in brackets. The total number of melt events is $N = 77$.

	Dur. [d]	**ME [m]**	**Max. T2M @ME [°C]**	**Min. melt extent [%]**	**Max. melt extent [%]**
Avg. $\pm \sigma$	4.1 $\pm$ 3.4	2692 $\pm$ 193	-0.2 $\pm$ 1.3	8.7 $\pm$ 5.2	44.6 $\pm$ 10.7
Min.	1.25	2333	-2.6 [2826 m]	1.2	29.0
Max.	16.25	3175	+5.0 [2637 m]	25.6	94.8

Table 3. The ERA-Interim variables traced along the 8-day backward trajectories ("Lagrangian variables").

Lagrangian variables		
abbreviation	**variable name**	**unit**
MASK	ice mask of the GrIS [0,1]	[ ]
T	temperature	[°C]
θ	potential temperature	[K]
θ_{cl}	1979–2017 potential temperature climatology	[K]
SKT	skin temperature	[K]
q	specific humidity	[g kg^{-1}]

(Eq. 1) numerically.

$$\frac{D\mathbf{x}}{Dt} = \mathbf{u}(\mathbf{x}) \tag{1}$$

where **x** is the position of an individual air parcel and **u** the 3D wind vector. We use 3D ERA-Interim wind fields to calculate kinematic backward trajectories from pre-defined starting locations and trace a set of variables along the trajectories (Table 3). In the domain defined by the 519 ice grid points (Sect. 2.2) trajectories are started equidistantly every 80 km in the horizontal~~.~~ , resulting in 267 starting points per height level. Most of the trajectory starting points are located over the GrIS accumulation zone, as 90%, 76%, and 56% of the starting points' ground level lies above 1000 m, 1500 m, and 2000 m, respectively. In the vertical, trajectories start at three near-surface layers in the lowermost ~500 m of the atmosphere (20, 40 and 60 hPa above ground level~~, i. e., from the lowermost ~500 m of the atmosphere, resulting in 3 × 267 starting points~~), representing air masses that exert a strong surface forcing. During the evaluation, we consider trajectories from all three layers to get a more robust estimate of the properties of typical air masses near the GrIS. The trajectories are calculated eight days backward in time and start every 6 h during a melt event. For smoother plotting, trajectory positions and all variables are written out every 3 h along the trajectories. One application of the trajectories is to perform so-called Lagrangian forward projections (LFP; Liniger and Davies, 2003; Sodemann et al., 2008), i.e., certain properties of the air mass, such as for example the total 8-day adiabatic warming, are projected onto the trajectory starting point above Greenland.

2.4 Lagrangian evaluation of thermodynamic energy equation

We evaluate the thermodynamic energy equation in order to get insight into the warming mechanisms along trajectories.

$$\frac{DT}{Dt} = \frac{\kappa T \omega}{p} + H \left(\frac{p_0}{p} \right)^{-\kappa} \tag{2}$$

According to Holton and Hakim (2012) and Bieli et al. (2015), the relationship between temperature, vertical motion, and diabatic processes (Eq. 2) follows from the thermodynamic energy equation and the material derivative of potential temperature $\theta = T(p_0/p)^{\kappa}$ [K], with reference pressure p_0 and $\kappa = R/c_p = 0.286$. The total diabatic heating rate is $H = D\theta/Dt$ [K s^{-1}], and the vertical velocity equals $\omega = Dp/Dt$ [Pa s^{-1}].

$$\Delta T = T_{adi} + T_{diab} \tag{3}$$

We split the warming integrated along the eight-day trajectories, ΔT, into adiabatic (Eq. 2, 1st term on r.h.s.) and diabatic (Eq. 2, 2nd term on r.h.s.) components (Eq. 3). The diabatic change of temperature along the trajectory is calculated from θ and p with the numerical approximation in Eq. 4. The adiabatic warming then follows as a residuum from this term and the total ΔT along the trajectory (Eq. 3).

$$\Delta T_{diab} = \sum_{t \in \{-189\,\mathrm{h}, \ldots, -3\,\mathrm{h}, 0\,\mathrm{h}\}} \frac{\theta(t) - \theta(t - 3\,\mathrm{h})}{3\,\mathrm{h}} \left(\frac{p_0}{0.5 \cdot (p(t) + p(t - 3\,\mathrm{h}))} \right)^{-\kappa} \tag{4}$$

Adiabatic warming/cooling is a consequence of adiabatic compression/expansion due to vertical motion (ω). We expect diabatic heating (H) to be dominated by radiative clear-sky cooling at $\sim$1 K d^{-1} (Cavallo and Hakim, 2013; Papritz and Spengler, 2017) and latent heating/cooling by condensation of water vapor or evaporation/sublimation of hydrometeors in and below clouds. Oceanic surface sensible heat fluxes in the midlatitudes are typically reduced in summer compared to winter and can only affect the few airstreams travelling in the surface layer.

3 Detailed analysis of melt event EV69

In order to illustrate our methodology and the processes at play, we start with a detailed case study of the EV69 melt event. It lasted from 18 UTC 2 July to 18 UTC 17 July 2012 and included the most extreme period of surface melt in terms of elevation (up to the highest grid cell at 3175 m) and maximum coverage (94.8%) on 12 July.

3.1 Synoptic situation

The synoptic flow configuration during EV69 was characterized by an exceptionally strong 500 hPa geopotential height anomaly, *Z500′*, over and near Greenland (Figs. 1a, c), and can be divided in two distinct periods of about one week each. The first period was initiated by the deepening of a slowly propagating low pressure system near Newfoundland (not shown) and an amplifying upper-level ridge over the Central North Atlantic. During the subsequent eight days, from 18 UTC 2 July to 12 UTC 10 July, the North Atlantic circulation pattern resembled a typical Omega-blocking (e.g. Woollings et al., 2018), as

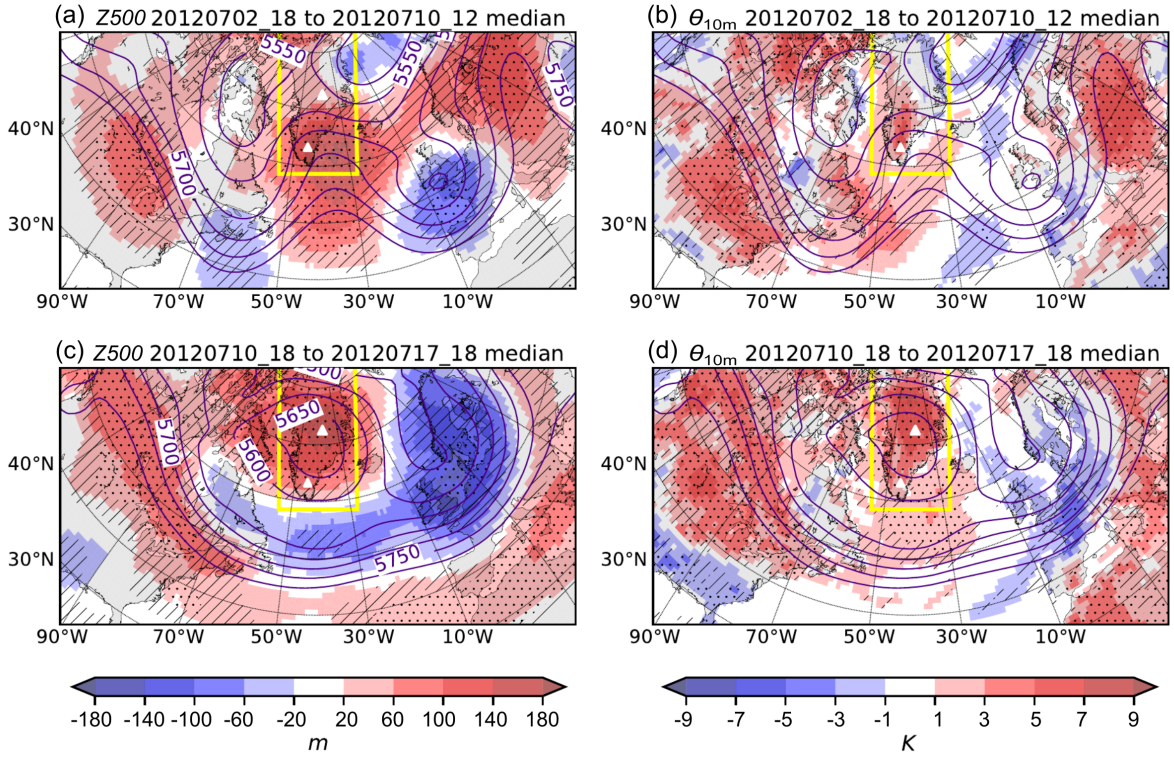

Figure 1. The median fields of 500 hPa geopotential height (*Z500*; contours) for the two periods during EV69 (a, b) 18 UTC 2 July to 12 UTC 10 July (8 days) and (c, d) 18 UTC 10 July to 18 UTC 17 July (7.25 days). Median anomalies of the synoptic fields in the respective periods are shown in colors (a, c) *Z500* and (b, d) near-surface potential temperature (θ_{10m}). Hatching (stippling) indicates an anomaly outside the 25–75 (10–90) percentile range of equally long periods in JJA 1979–2017. The yellow box indicates the location of the GrIS.

evident from the shape of the *Z500* contours (Fig. 1a). High values of *Z500* located southeast of Greenland, with an anomaly vastly above the 90th percentile, were sustained and stabilized by an upstream trough over Newfoundland and a downstream trough over the UK. Another strong ridge was present further downstream over Russia (Fig. 1a). In the lower troposphere, the southerly flow between the upstream low and the Greenland ridge advected exceptionally warm air to southern and western Greenland, causing near-surface potential temperature anomalies, θ'_{10m}, of more than 5 K, as well as to neighbouring regions such as Newfoundland, the Labrador Sea and Baffin Bay (Fig. 1b). Another striking feature is the exceptional heat wave of similar anomaly magnitude over the Great Plains of North America (Hoerling et al., 2014; Neff et al., 2014).

By the end of the first period, the positive $Z500'$ migrated poleward. Thus, the circulation during the second half of EV69, the 7.25-day period from 18 UTC 10 July to 18 UTC 17 July, was characterized by a less meridional flow south of Greenland and a cut-off anticyclone centered over the GrIS, while a deep trough dominated over northern Europe (Fig. 1c). The median $Z500'$ over Greenland during this period was around +150 m (>90th percentile), except for the southern tip of the GrIS. It went

along with an equally exceptional θ'_{10m} over the GrIS and the northeastern North Atlantic, peaking in northern Greenland with values of >+7 K (Fig. 1d).

The combination of the cyclone over Newfoundland and the anticyclone over the GrIS favoured northward transport of low-level air masses from the subtropical North Atlantic towards the southern tip of Greenland and the Labrador Sea. Figure 2 shows air masses arriving over the GrIS during melt time steps - hereafter referred to as "melt air masses". Several distinct streams of melt air masses can be identified: Two airstreams originating close to the east coast of North America ascended over the southern tip of Greenland into the mid-troposphere and descended anticyclonically onto the central and eastern GrIS (labels C, E). Another important contribution stemmed from the subtropical North Atlantic. These airstreams followed a northward trajectory also towards southern Greenland, where the higher air masses ascended slightly to reach Southdome in a straight trajectory (S), whereas those in the marine boundary layer moved into the Labrador Sea and from there - remaining at low altitudes - further northward to reach the northern GrIS in a final rapid ascent (N1). It is interesting to note that the bulk of N1 air parcels did not ascend along Greenland's west coast but instead remained at low levels until they approached Northwest Greenland. An additional airstream reached the North at lower altitudes from neighbouring regions and approached the GrIS from the Northwest (N2)~~or descended in the dry intrusion of the~~ , or descended cyclonically in the low near Newfoundland. Hereafter, we refer by C, E, N, S, or W air masses to air masses arriving in the specific region, irrespective of whether they follow a similar trajectory as shown in the previsouly discussed example (Fig. 2).

3.2 Lagrangian forward projection

The Lagrangian analysis is split in two parts in which we identify (i) sources of air masses (Sect. 3.2.1) and (ii) mechanisms (Sect. 3.2.2) that contributed to surface ice melt over the GrIS prior to or during EV69; specifically, we consider the characteristics of the air mass origin and the following transport focusing on thermodynamic temperature changes along the trajectories.

3.2.1 Air mass origin

By comparing with the climatological characteristics of air masses arriving over the GrIS, we pinpoint the anomalous nature of the EV69 melt trajectories in terms of latitude, altitude and temperature anomaly. For each melt trajectory we define the relative minimum latitude and relative minimum pressure as the differences between the respective values of latitude and pressure at the destination over the GrIS and the minimum values along the trajectory, thus, indicating the largest changes in latitude and pressure. To that end, we make use of 8-day backward trajectories from the lowermost 60 hPa above the GrIS (see Sect. 2.3) during melt time steps associated with EV69. Figures 3a, c show the relative minimum latitude and pressure projected onto the trajectory starting locations over the GrIS in a so-called Lagrangian forward projection. In addition, we show their anomalies with respect to the climatological reference defined as all air parcels that arrived over the GrIS during JJA 1979–2017, i.e., typical values for all summertime air masses that arrive over the GrIS (Figs. 3b, d).

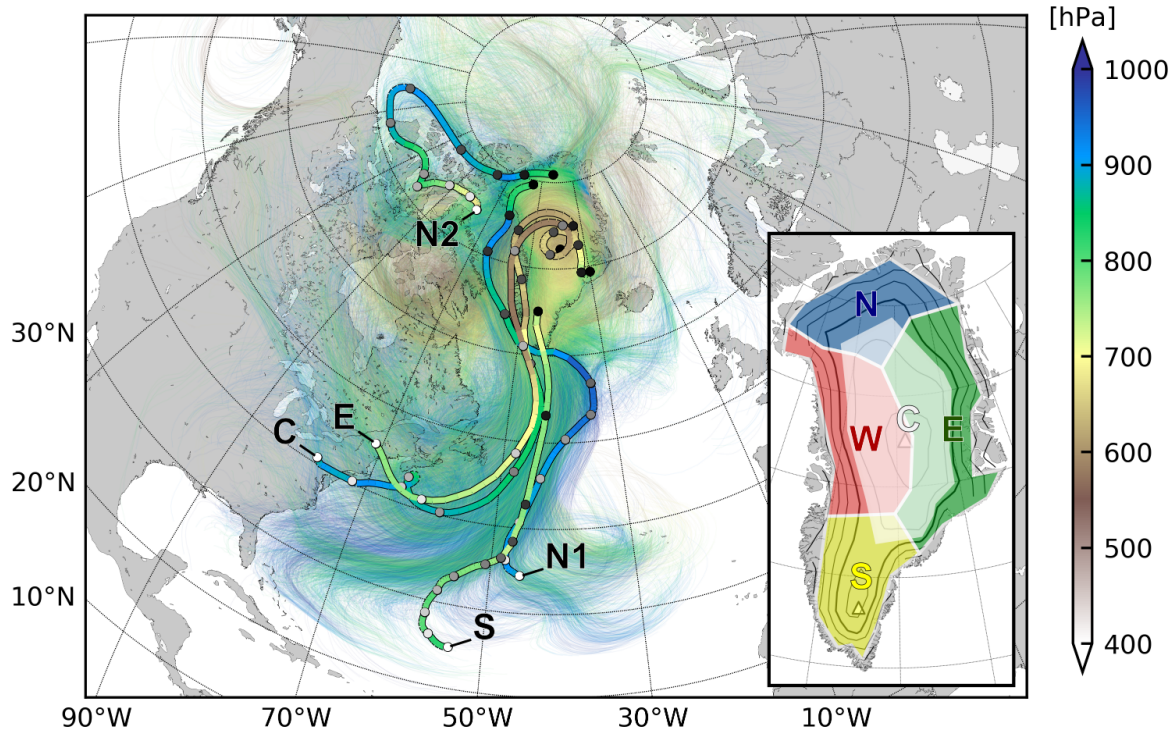

Figure 2. All extended (10-day) melt trajectories of EV69 colored according to their pressure. Five representative example trajectories represent characteristic airstreams (S, C, E, N1, N2), shown in thicker lines with one circle per day colored from white ($t = -240$ h) to black ($t = 0$ h). The subfigure map shows characteristic regions of the GrIS: South (S), West (W), North (N), East (E), and central plateau (C).

Generally speaking, the median melt air mass moved poleward by about 20° latitude in region S and up to 40° latitude in region N (Fig. 3a). Thus, it originated from a region in the atmosphere located around 20° latitude further south wrt. climatology (Fig. 3b). In addition, it descended by about 50 hPa less than the climatological air parcels, which applies, in particular, to Southdome and the region N (Fig. 3d). In fact, many melt air masses arriving in these regions show a relative minimum pressure of less than 20 hPa, meaning that they had never reached far above their final elevation and hence ascended from the lowermost parts of the troposphere (Fig. 3c). Further, most air parcels show initially, at $t = 192$ h, a small potential temperature anomaly wrt. the local climatology, θ_{cl}, of ∼0.5–2.5 K, which is highly unusual compared to the average air mass, which shows an approximately 0 K initial anomaly (Fig. S1c). The origin of these initial warm anomalies is related to the North American heat wave (Hoerling et al., 2014) and other anomalously warm source regions, predominantly in the Canadian Arctic. An interesting exception concerns melt air masses reaching region N, which did not come from regions with a positive temperature anomaly. They, however, show the largest relative minimum latitude, i.e., strongest meridional transport, of more than 40° latitude (Fig. 3a). Other exceptional melt air masses arrived over regions C and E, showing slightly increased descent compared to the climatological air masses (Fig. 3d).

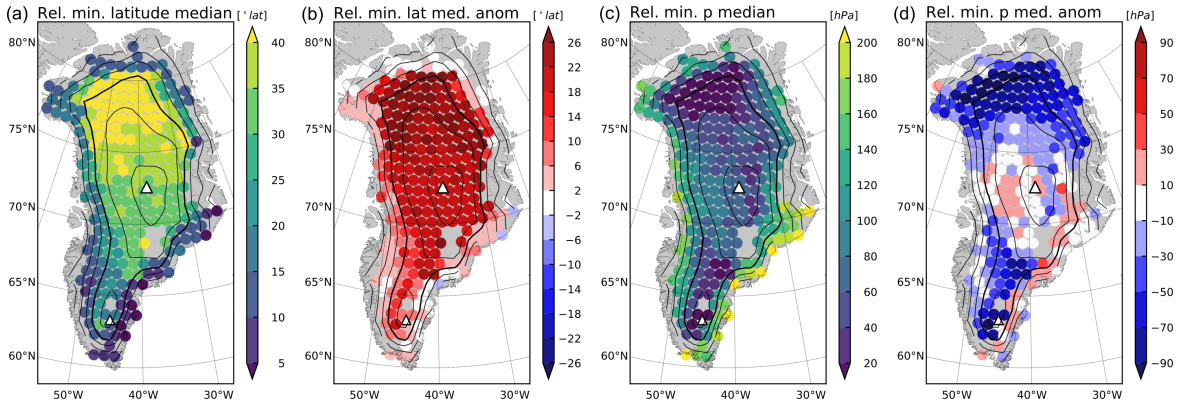

Figure 3. Lagrangian forward projection (LFP) of the median (a) relative minimum latitude, (c) relative minimum pressure (where positive values mean from (a) lower latitudes and (c) above), and (b, d) the respective anomaly fields of 8-day melt trajectories of EV69 wrt. the climatological summertime air parcels. The contours indicate elevation in 500 m intervals with the 2000 m isoline in solid. Summit and Southdome are marked with triangles.

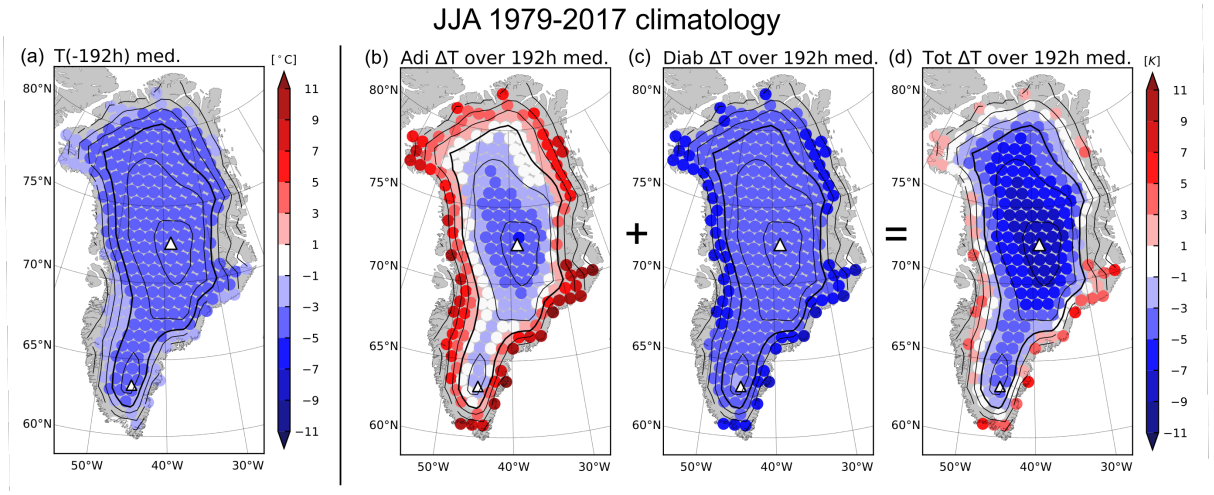

Figure 4. LFP maps as in Fig. 3 of the (a) initial temperature at $t = -192$ h, and (b) adiabatic, (c) diabatic, and (d) total temperature change over eight days and of the JJA 1979–2017 climatological summertime air masses.

3.2.2 Air mass evolution

In order to assess the relative importance of adiabatic and diabatic temperature changes for the final temperature anomalies of
245 EV69 melt air masses, we first consider the typical temperature evolution of all air parcels that arrive over the GrIS during JJA 1979–2017. The initial temperature is very uniform for all trajectories with a median of $T = -3.8$°C at $t = -192$ h (Fig. 4a). While in the following all air parcels experience diabatic cooling of about 0.5–1 K day^{-1} (Fig. 4c), mostly due to longwave

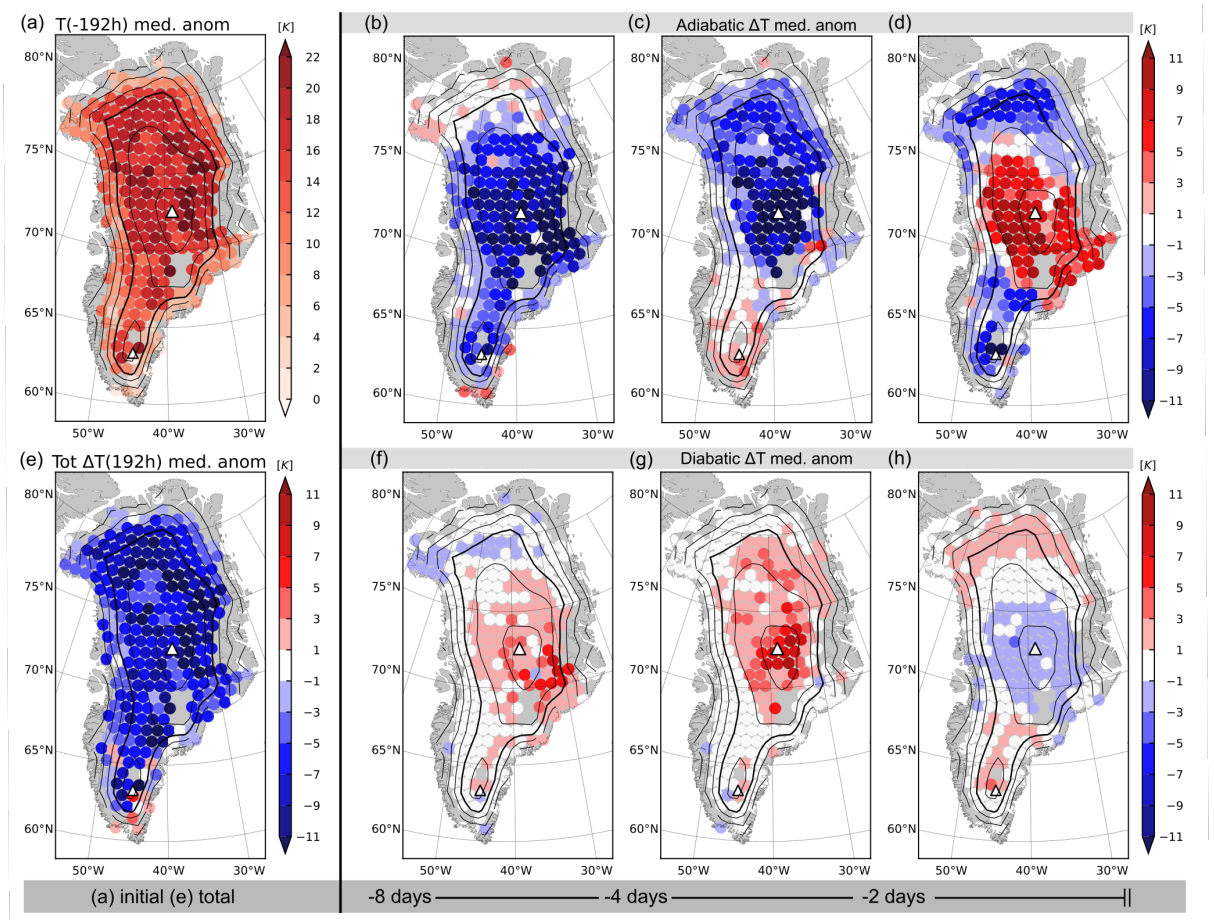

Figure 5. LFP anomaly maps of the (a) initial temperature at $t = -192$ h, and (b–d) adiabatic, (f–h) diabatic, and (e) total temperature change over eight days wrt. the climatological summertime air masses shown in Fig. 4. The adiabatic and diabatic temperature change anomalies are split up in the periods (b, f) $t = -192$ h to $t = -96$ h, (c, g) $t = -96$ h to $t = -48$ h, and (d, h) $t = -48$ h to $t = 0$ h.

radiative fluxes, the adiabatic temperature changes exhibit a strong elevation dependence. Specifically, C air masses cool adiabatically, indicating ascent prior to arrival over the GrIS (Fig. 4b). Air masses arriving in ~~the coastal areas~~or closer to the ablation zone, in contrast, experience overall adiabatic warming. This descent is likely the result of katabatic drainage flows prevalent over the GrIS (cf. Heinemann and Klein, 2002). Consequently, cooling dominates the temperature evolution of most air masses arriving over the elevated regions of the GrIS, whereas at lower elevations adiabatic warming compensates for much of the radiative cooling such that these air masses experience little to slightly positive overall temperature changes (Fig. 4d). Except for some of the latter, summertime air parcels arrive with negative temperatures within the lowermost 60 hPa (∼500 m) aloft the GrIS, because of $T < 0$°C at $t = 192$ h (Fig. 4a) and cooling during the transport to Greenland (Fig. 4d).

The adiabatic and diabatic temperature modifications of EV69 melt air masses deviated from the typical summer air mass as shown in Fig. 4. At the start of their trajectory ($t = -192$ h), melt air masses were about 10–16 K warmer than climatological air masses (Fig. 5a). Melt air masses arriving ~~closer to the coast~~ at lower elevations or even the ablation zone of Greenland showed a smaller initial temperature anomaly (T'<+10 K) than those arriving in region C (T'>+16 K). From the evolution during the subsequent eight days, we again refer to representative melt airstreams with different characteristics (see Fig. 2): a melt airstream arriving over (i) the central plateau and East Greenland ("C" and "E"), (ii) North Greenland ("N1", "N2"), and (iii) South Greenland (including Southdome; "S"), respectively. Figures 5b–d and f–h show the adiabatic and diabatic temperature changes during days 0–4, 5–6, and the last two days of the transport to Greenland. N air masses exhibited a thermodynamic evolution in the beginning that was close to that of the climatological air masses (Figs. 5b, f) and an orographically induced final ascent reflected in enhanced adiabatic cooling (Figs. 5c, d). In close proximity to the GrIS, N air parcels ascended from the South (N1 in Fig. 2) or the West (N2 in Fig. 2) to the northern GrIS. Airstream S showed a similar pathway as N1 but with initially exceptional adiabatic cooling before reaching Greenland (Fig. 5b) and subsequently orographic ascent from the South (Fig. 5d). The associated adiabatic cooling and diabatic warming were less pronounced and occurred later in S compared to N (Figs. 5c, d, g, h).

Airstreams C and E experienced much stronger than usual adiabatic cooling during most of the 8-day period, especially between $t = -144$ h and -48 h, which indicates enhanced ascent (Figs. 5b, c). This ascent either stemmed from dynamical lifting at the polar front, i.e., by the trough over Newfoundland (C in Fig. 2), and/or orographic lifting at the southern tip of Greenland (E in Fig. 2; cf. Stohl, 2006). Interestingly, during the final 48 h, these airstreams experienced strong adiabatic warming due to descent onto the GrIS. Over eight days, the total adiabatic warming anomaly is typically below -10 K and diabatic heating in melt air masses is anomalous by +5 K - both signals especially distinct in airstreams C and E. The total temperature change was uniform over the GrIS and its GrIS-wide median equaled -6.2 K (Fig. 5e), with the initially warmest air masses (Fig. 5a) cooling more than the rest. Nevertheless, 40–80% of the initial warm temperature anomaly of the melt air masses wrt. the climatological air masses (Fig. 5a) was sustained and not compensated by stronger cooling than along the climatological trajectories.

Previous studies (Neff et al., 2014; Bonne et al., 2015) have shown that anomalously warm and humid air masses associated with the heat wave over North America contributed to EV69. To quantify this contribution, we extend our set of backward trajectories to ten days and define heat wave trajectories as those melt trajectories that (i) pass the North American Great Plains at some point, and (ii) at the same time have a potential temperature anomaly wrt. θ_{cl} in excess of 3 K. The fraction of these trajectories among all melt trajectories is shown in Figs. 6a, b. The highest contributions of heat wave air masses ~~are found for airstreams~~ end in the upper accumulation zone of regions C and E (up to 70% near Summit; C and E in Fig. 2). The heat wave trajectories ending at locations with more than 60% U.S. heat wave contribution were initially anomalously warm (also constrained by the selection criteria) and had a high specific humidity of $\sim$8 g kg^{-1} (Fig. 6c). During their way from the American continent to the western North Atlantic (until $t = -120$ h), however, these air masses lost most of their warm anomaly. This is in contrast to the idea that they carried the original temperature anomaly from North America to Greenland. At the same time,

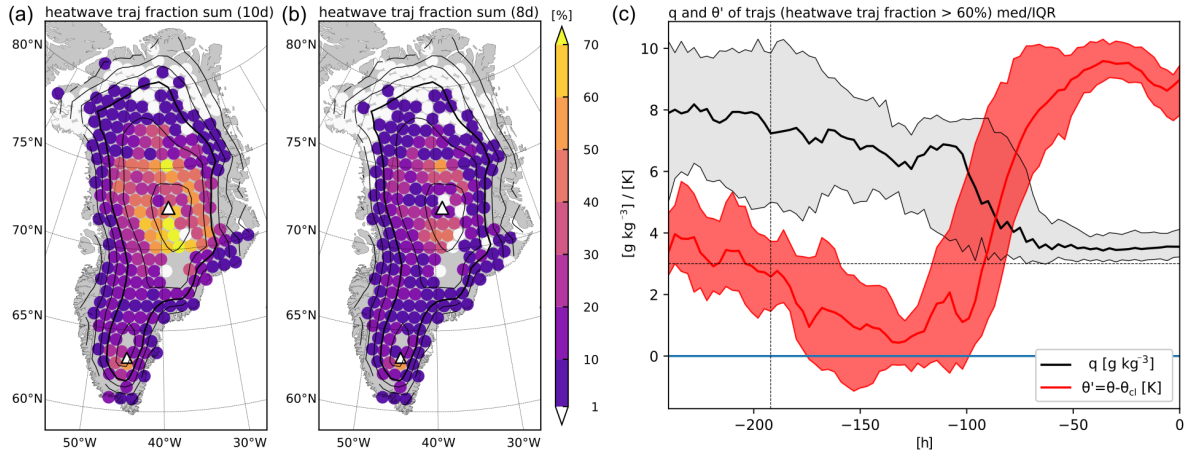

Figure 6. LFP maps of the trajectory fraction being associated with the North American heat wave (see text for details), for (a) the extended 10-day or (b) 8-day trajectories; (c) shows the median (solid line) and inter-quartile range (shading) of specific humidity q (grey) and θ' wrt. θ_{cl} (red) of heat wave trajectories ending at locations with a heat wave trajectory fraction >60%. Dashed lines in (c) indicate $t = -192$ h and $\theta' = +3$ K.

they conserved their moisture to a large degree, with the driest ones picking up additional moisture once they reached the open ocean. It is only between $t = -120$ h to -48 h when the air masses rapidly moved poleward into a climatologically much colder region that their warm anomaly increased from around +1 K to almost +10 K. The concurrent reduction of specific humidity confirms the condensation of water vapour and aforementioned diabatic warming during that period (Figs. 5f, g), which was linked to ascent along the sloping isentropes as the air mass moved poleward. Indeed, air masses came from the U.S. heat wave but the temperature anomaly near the origin of their trajectories was not directly responsible for the warm anomaly upon arrival in Greenland.

In summary, we conclude that exceptional poleward transport and ascent of relatively moist and climatologically warm air masses contributed substantially to EV69 by advection towards the climatologically much colder GrIS region. Nevertheless, air masses leading to this ~~Greenland~~ large-scale melt event were cooled stronger than usual during their transport to the GrIS. In these warm, moist and poleward ascending airstreams, ~~cloud formation and latent heating~~ latent heating from condensation of water vapour compensated some of the adiabtic cooling and contributed to the warm anomaly over the GrIS.

3.3 Linkage to clouds and radiative effects

The characteristic airstreams during EV69 (C, E, N1, N2, S; Fig. 2) likely played an important role in modulating the spatial distributions of rain and snowfall, cloud liquid water, and radiative fluxes over the GrIS, which in turn had a strong impact on the melt potential. To illustrate these inter-linkages, we consider rain rate (*RR*), total column liquid water (*TCLW*), sur-

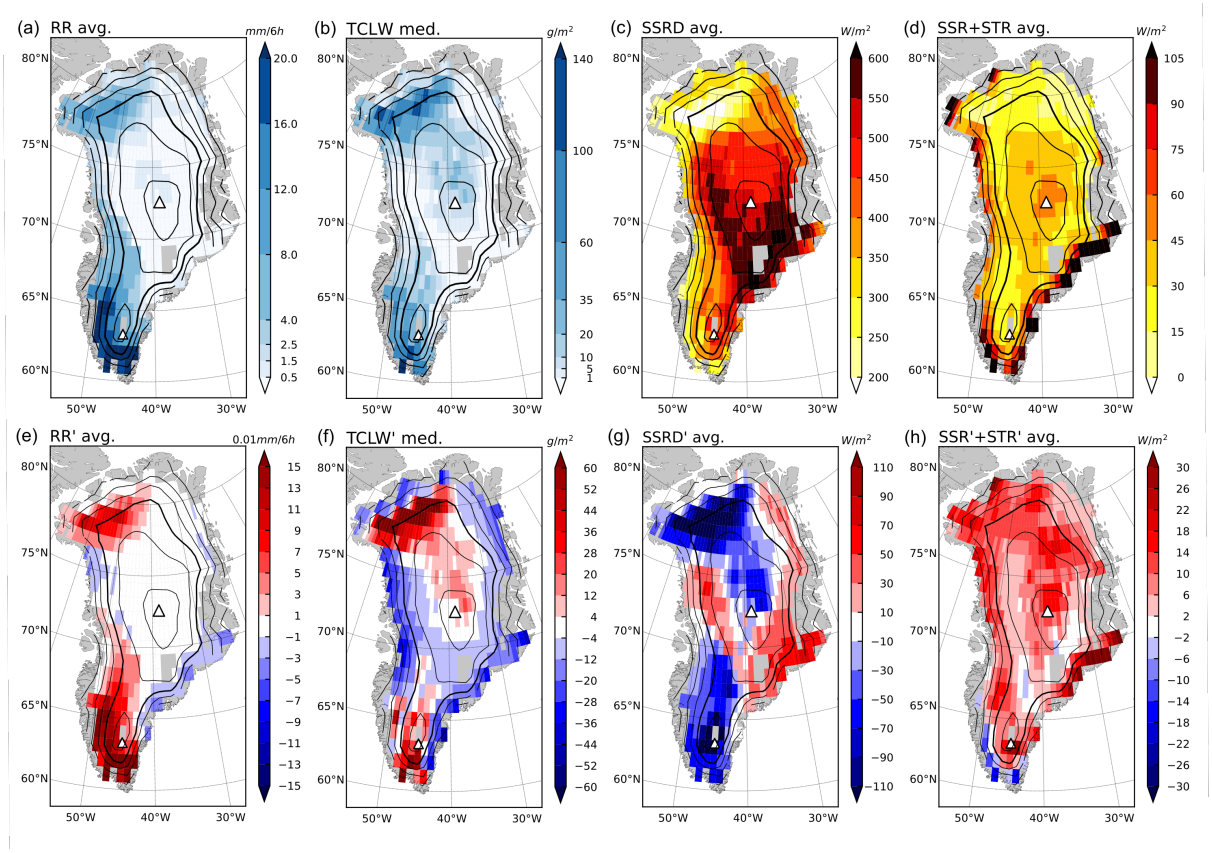

Figure 7. Composites of (a) rainfall (*RR*), (b) total column liquid water (*TCLW*), (c) surface shortwave downward radiation (*SSRD*), (d) net surface long- and shortwave radiation (*SSR+STR*) during EV69 melt time steps, and (e–h) the respective anomalies wrt. climatology. Depending on the melt impact of the variable, the composite results from the average (*RR, SSRD, SSR+STR*) or the median (*TCLW*). The contours indicate elevation in 500 m intervals with the 2000 m isoline in solid. Summit and Southdome are marked with triangles.

face shortwave downward radiation (*SSRD*) and the sum of net surface short- and longwave (thermal) radiation (*SSR+STR*;
310 Figs. 7a–d), as well as their anomalies wrt. the 1979–2017 summer climatology (Figs. 7e–h) for melt time steps at the respective grid points. We note that our results are based on the specific selection of large-scale melt events (Sect. 2.2) and ERA-Interim, whose resolution (∼100 km) is not resolving the narrow (20 – 100 km) ablation zone topography and surface processes correctly, i.e., mainly address characteristics of the accumulation zone. Still, the investigated variables and effects are relatively well represented in the Arctic in ERA-Interim (Wesslén et al., 2014; Wang et al., 2019).

315

Figure 7 indicates distinctive patterns over the GrIS that are related to the pathways of and processes within air masses arriving on the GrIS during EV69. The ascending airstreams S, N1, and N2 were associated with strong anomalies of *TCLW* and rainfall in southern and north-western Greenland, respectively (Figs. 7a, b, e, f). In particular, airstream N1 carried moisture

far northward and, as it ascended onto the GrIS north of Summit, the air parcels reached saturation. Consequently, *TCLW* and *RR* exceeded their climatologies in the entire region N. Similarly, also region S experienced strong *TCLW* and *RR* anomalies due to the ascending airstream S. Interestingly, in region W, *TCLW* and *RR* were below average. This is related to the fact that the humid air masses associated with airstream N1 remained in the boundary layer and did not ascend until they reached northwestern Greenland. Consequently, the air masses arriving in region W were transported at higher levels than airstream N1 and did not ascend or may even have experienced slight descent, thus leading to cloud-free conditions. Regions with precipitation experienced an additional heat flux into the ice from rain, while snowfall and total column ice water were widely reduced (Fig. ~~S2b~~S3b), as was previously highlighted by Doyle et al. (2015) and Fausto et al. (2016). In direct relation to increased *TCLW*, *SSRD* was strongly reduced, especially in region N (Figs. 7c, g). In contrast in regions E and W, clear-sky conditions with hardly any precipitation prevailed (Fig. 7a), as evident from extremely low *TCLW* (Fig. 7b), as well as substantially increased *SSRD* (Fig. 7g). Southeast of the plateau, this relates to the branch of the descending airstreams C and E that stretched anticyclonically from west to east across the central portion of the GrIS.

Despite the reduction in downwelling shortwave radiation in the regions with above average *TCLW*, the sum of net short- and longwave radiation was positive across the entire GrIS accumulation zone (Fig. 7d)~~and almost everywhere~~ , and in excess of climatological values (Fig. 7h). This is in part explained by enhanced downwelling longwave radiation in the cloudy regions. There and also at and north of Summit, the shift of the cloud phase to the liquid regime was found to be decisive for the observed melt (Bennartz et al., 2013; Solomon et al., 2017). In addition, also total column water vapour was above the long-term summer climatology over all of the GrIS accumulation zone (area-weighted average anomaly of +3.3 $\mathrm{kg\,m^{-2}}$; Fig. ~~S2f~~S3f). The area-weighted GrIS-wide average anomaly of *SSR+STR* (Fig. 7h) amounted to +9.4 $\mathrm{W\,m^{-2}}$ and provided additional energy corresponding to a melting potential of 2.7 $\mathrm{cm\,ice\,d^{-1}}$ (resulting from the heat of fusion of water, 333.55 $\mathrm{J\,g^{-1}}$, and assuming ice at 0°C with a density of 917 $\mathrm{kg\,m^{-3}}$).

4 Climatological analysis for melt events in 1979–2017

In this section we generalize the results from the EV69 case study by considering all 77 ~~Greenland~~ large-scale melt events. We present the synoptic situation during ~~Greenland~~ large-scale melt events (Sect. 4.1), the air masses associated with these events and their temperature modifications (Sect. 4.2), and finally precipitation, moisture, and radiation patterns over the GrIS accumulation zone and its subregions (Sect. 4.3).

4.1 Synoptic situation

We illustrate the synoptic situation related to ~~all Greenland~~ melt events in 1979–2017 by compositing *Z500* and its anomaly field, *Z500′*, relative to climatology (Fig. 8). The composites are calculated five and two days prior to the melt time steps, at the melt time steps, and five days later. It is important to note that some of the time steps entering lagged composites were themselves part of the respective melt event if the melt criterion is satisfied also at the lagged time. As for EV69, melt events

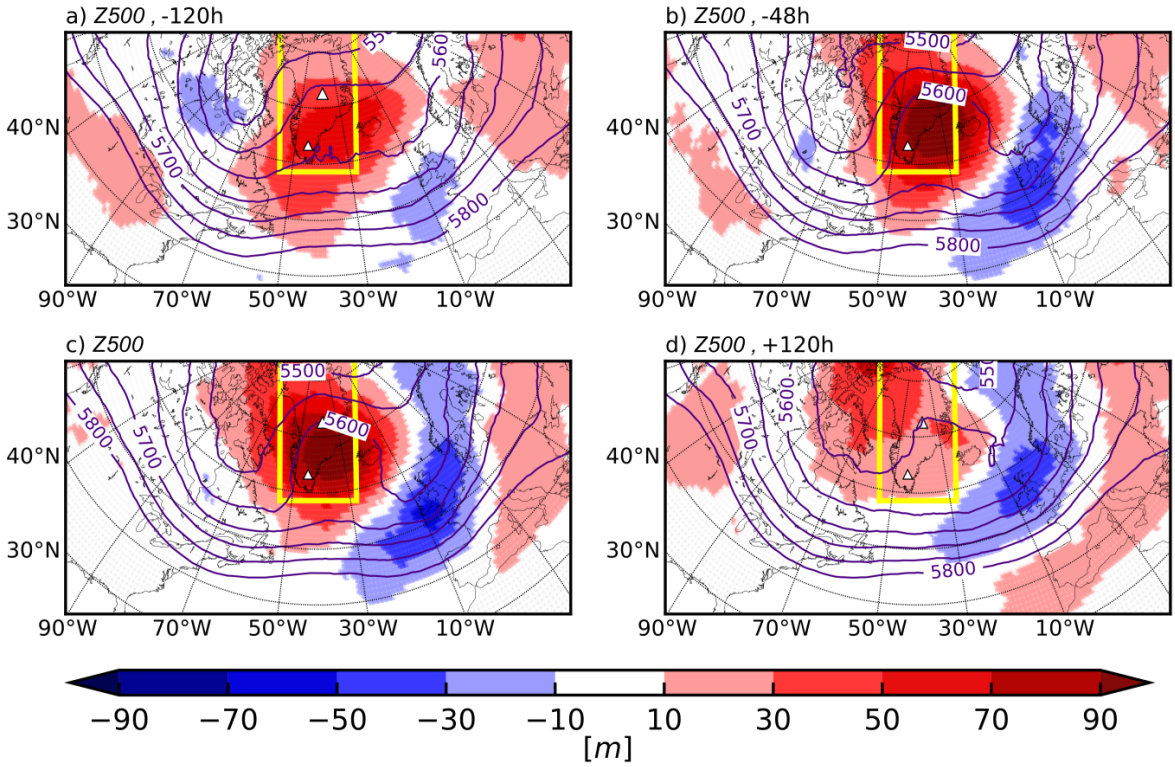

Figure 8. Median composites of 500 hPa geopotential height (*Z500*) in contours and their anomalies wrt. climatology in colors for different lags relative to all melt event time steps: (a) $lag = -120$ h, (b) $lag = -48$ h, (c) $lag = 0$ h, and (d) $lag = +120$ h. The yellow box indicates the location of the GrIS.

are characterized by a dipole pattern of *Z500′* with a positive anomaly centered over southeastern Greenland and a pronounced negative anomaly over northern Europe. A positive *Z500′* of +50–70 m is typically present already 120 h before melt occurs, accompanied by troughs both upstream and downstream. This initial pattern is, thus, akin to the geopotential height anomalies associated with cyclonic Rossby wave breaking and omega-type blocking (Fig. 8a; Liu and Barnes, 2015). Towards $lag = 0$ h, the anomalies transition into the dipole pattern with a strong ridge or cut-off anticyclone over Greenland and a pronounced trough over the British Isles and Scandinavia (Figs. 8b, c). *Z500′* near Greenland peak at >+90 m around 24 h before melt occurs. Five days after a melt event, the positive *Z500′* has shifted towards northwestern Greenland and the high Arctic (Fig. 8d). The dipole pattern is characteristic of the Greenland blocking regime (e.g., Grams et al., 2017), which projects negatively onto the NAO index and positively onto the GBI.

This synoptic configuration provides favourable conditions for the poleward advection of warm and moist air masses from lower latitudes towards Greenland (Liu and Barnes, 2015), as reflected in the enhanced total column horizontal water vapour

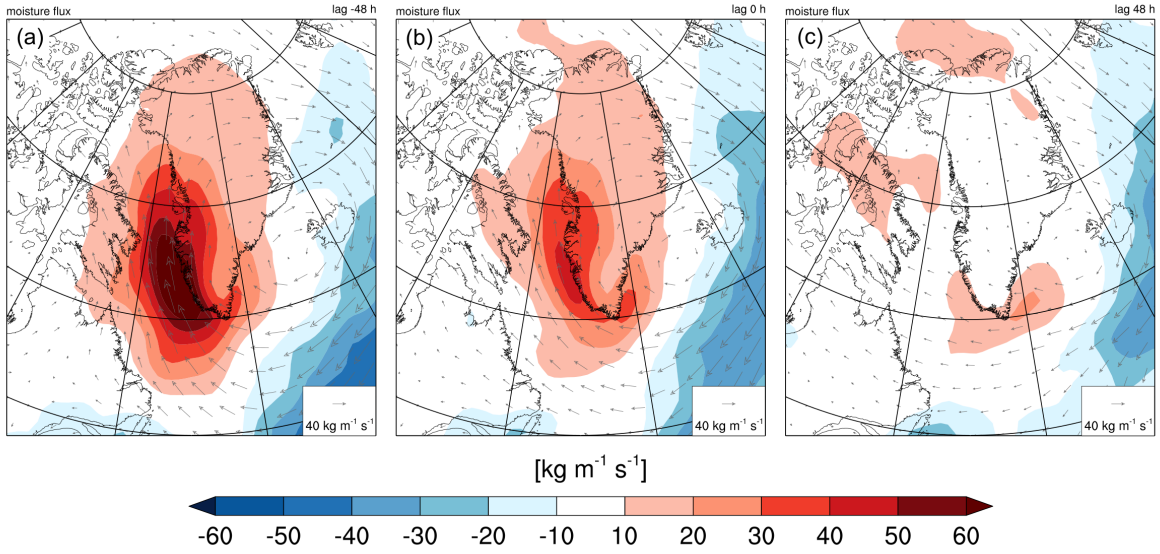

Figure 9. Median composites of total column horizontal water vapour transport anomalies ($TCVHT'$) wrt. climatology for different lags relative to melt event time steps: (a) $lag = -48$ h, (b) $lag = 0$ h, and (c) $lag = +48$ h.

transport (*TCVHT*) especially along the southwestern GrIS (Fig. 9). The anomalous *TCVHT* starts over the Labrador Sea several days before the melt event (not shown) and the anomaly increases up to >+60 kg m^{-1} s^{-1} at $lag = -48$ h while at the same time reaching the northern and central GrIS (Fig. 9a). The anomaly then gradually fades and vanishes completely in line with the weakening *Z500′* after melt events (Figs. 9b, c). The centering of the positive geopotential height anomaly between southeastern Greenland and Iceland instead of over Greenland is a particularly important ingredient for the transport of moist-warm air parcels towards western Greenland and in an arc-shaped anticyclonic flow pattern across northwestern and northern Greenland, as discussed already for EV69.

4.2 Lagrangian forward projection

The analyses presented in the following are analogous to those for EV69 (Sect. 3.2), but now for all ~~Greenland~~ 77 large-scale melt events in JJA 1979–2017. Note, however, that melt at the most elevated parts of the GrIS is very rare, which is why the results near Summit strongly resemble those in EV69.

4.2.1 Air mass origin

Except for some arriving very high on the GrIS, at $t = -192$ h melt air masses are not anomalously warm compared to the local climatology θ_{cl} (Fig. S1a). They are, however, located much further south than usual, i.e., in a climatologically warmer region - more so for air masses arriving in region C and N and near Southdome (Fig. 10b). ~~Coastal air masses~~ Air masses reaching lower elevations previously move further poleward by 10° latitude and inland air masses by up to 26° latitude than

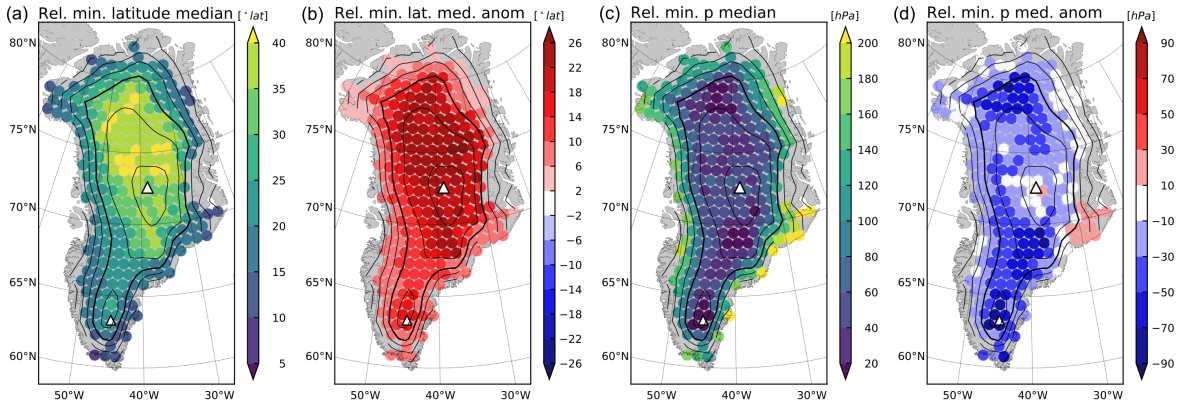

Figure 10. As Fig. 3 but for melt trajectories during all ~~Greenland~~ large-scale melt events.

normal summertime backward trajectories from these ~~location~~ locations (Fig. 10a). The primary origin of melt air masses lies southwest of the GrIS, predominantly the Canadian Arctic, but also over the subtropical North Atlantic (Fig. S2). A smaller amount of melt air masses approach Greenland from the East, including northern Europe - a rather exceptional transport pattern that reoccurred in summer 2019 with extreme mass loss (Tedesco and Fettweis, 2020). At the same time, the melt trajectories reach less high levels prior to arriving on the GrIS and, therefore, experience less subsidence than climatological air masses (Fig. 10d). Comparing spatial patterns in Fig. 10, we find that ~~, as during EV69,~~ air masses ending in regions C, E, N, and S (subfigure in Fig. 2) share very similar transport characteristics as during EV69 (Sect. 3.2). N and S air masses reach the maximum elevation of their entire 8-day trajectory once they reach the GrIS (Fig. 10c). The only melt air masses influenced by anomalously strong descent arrive in region E after - embedded in the anticyclonic flow - crossing the GrIS in an arc-like fashion (Fig. 10d).

4.2.2 Air mass evolution

Due to a climatologically warmer origin (lower elevation and/or lower latitude), ~~all~~ melt air masses are at $t = -192$ h warmer wrt. the climatological summertime air mass arriving at the same location (Fig. 11a). There are no substantial local temperature anomalies at $t = -192$ h (Fig. S1a). Thus, the positive anomalies of 10–20 K in Fig. 11a can be attributed to the unusual origin of air masses. The time series of adiabatic (Figs. 11b–d) and diabatic temperature change anomalies (Figs. 11f–h) along the trajectories during all large-scale melt events look very much alike the ones for EV69 (Sect. 3.2). C air masses ascend and cool adiabatically by a larger amount than the climatological air masses between $t = -144$ h to -48 h (Figs. 11b, c), while at the same time experiencing more diabatic heating (Figs. 11f, g). Furthermore, C and E air masses both show a stronger final descent reflected in enhanced adiabatic warming in the last two days (Fig. 11d). Finally, air masses ending in regions N and S ascend more wrt. the climatological summertime air masses within the last two days due to their advection towards sloping

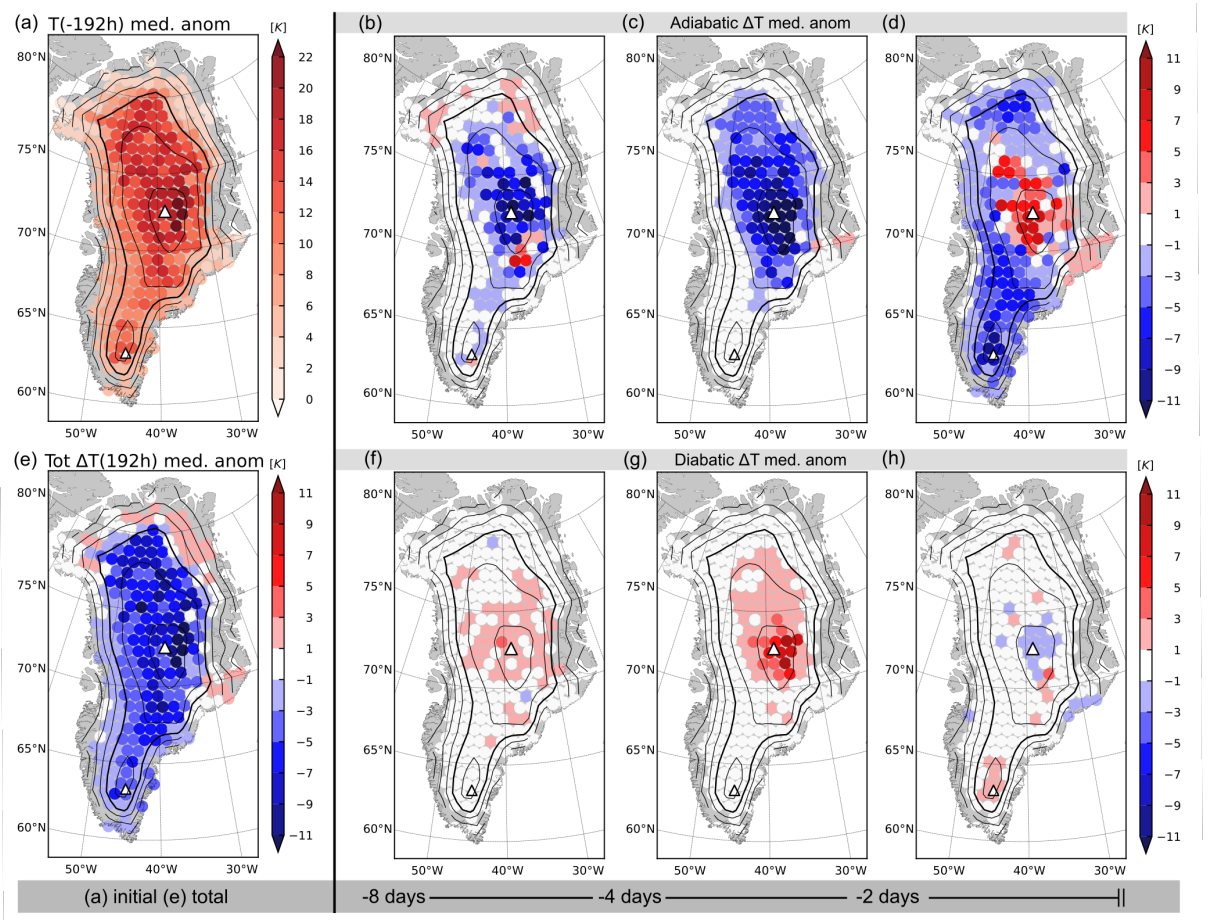

Figure 11. As Fig. 5 but for melt trajectories during all ~~Greenland~~ large-scale melt events.

orography, that is south- to northwesterly advection towards region N or southerly advection towards region S (Fig. 11d).

Overall, the anomalies are slightly weaker than for EV69 and show a stronger elevation dependency. Air masses at lower elevation have a thermodynamic history close to that of climatological air masses with slightly enhanced cooling for S, and enhanced warming for E and N air masses, respectively (Fig. 11e). In contrast, air masses ending in region C and near Southdome are more strongly cooled adiabatically, which is in part compensated by enhanced diabatic heating during the above-normal ascent. In total, however, most melt air masses experience stronger anomalous cooling during the eight-day period prior to arrival over the GrIS. As a consequence, only about 50-90 % of the higher initial temperature as seen in Fig. 11a remains when the air masses arrive on the GrIS.

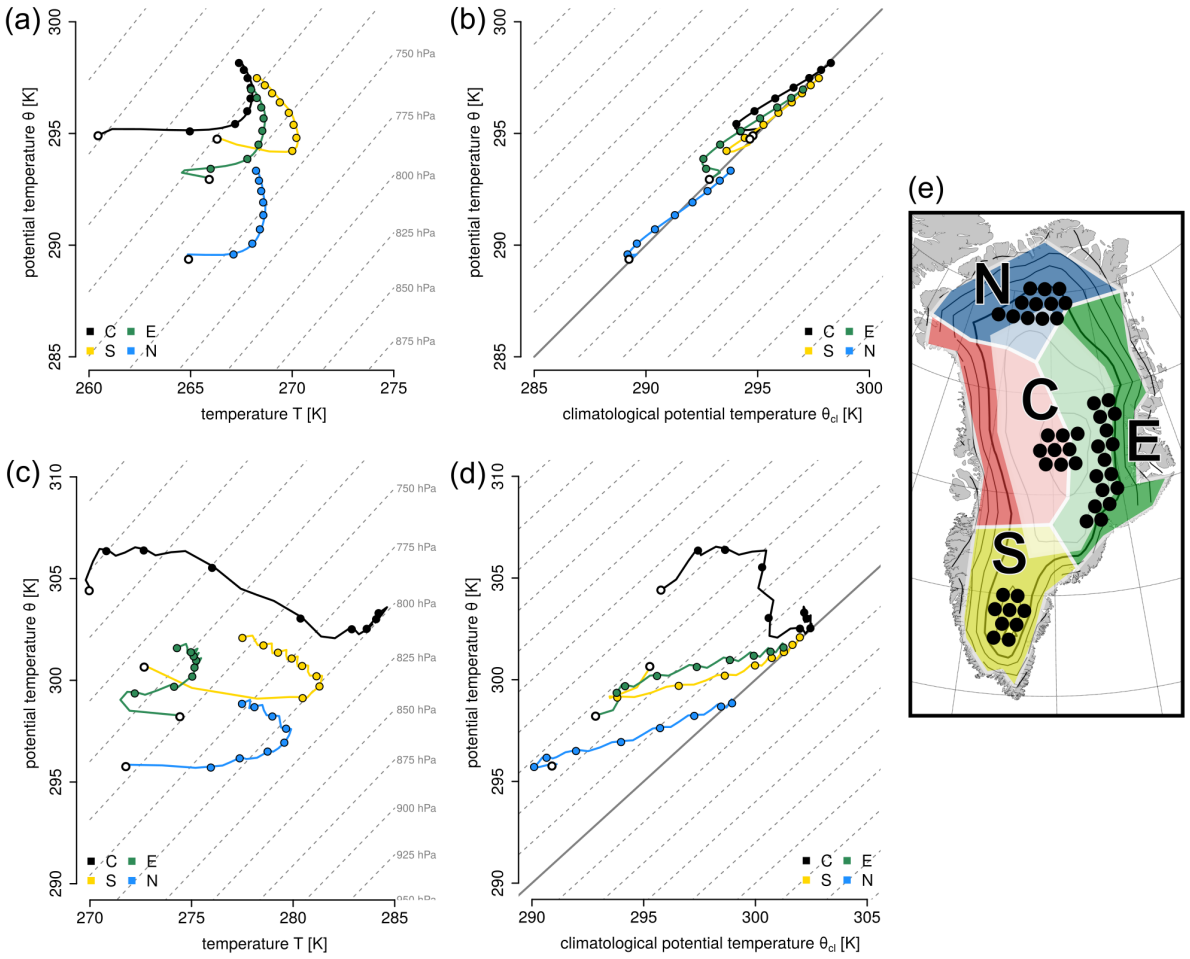

Figure 12. Thermodynamic evolution of backward trajectories from selected starting points (see panel e) representative of regions C, E, S, and N. Shown are medians for each trajectory category, summarized as one air parcel, in (a, c) $\theta - T$ and (b, d) $\theta - \theta_{cl}$ space. Grey dashed lines indicate isobars in intervals of 25 hPa (a, c) and isolines of constant potential temperature anomaly in intervals of 2 K (b, d). Panels (a, b) represent all climatological summertime air masses and (c, d) represent melt air masses only. Circles along the lines indicate time in 24-hour intervals, starting at $t = -192$ h and with an empty circle at the trajectory end point at $t = 0$ h. Note that the axis limits of plots (a–d) are not identical.

In line with the characteristic regions shown in Fig. 2 and the spatial patterns identified in Figs. 10 and 11, we select several trajectory starting points between 2000–2500 m altitude representative of air masses ending in regions E, S, and N (see Fig. 12e). Furthermore, for region C, we consider melt trajectories arriving above 2500 m altitude. In the following we will consider the evolution of T, θ, and θ_{cl} for trajectories arriving in each region. The air masses' evolution in $\theta - T$ space (Figs. 12a, c) gives insight into the contributions of adiabatic temperature changes associated with vertical motion (changes along horizontal axis) and diabatic processes (changes along vertical axis). Furthermore, the evolution in $\theta - \theta_{cl}$ space (Figs. 12b, d) indicates

when the final potential temperature anomalies emerge and it reveals the relative importance of transport from climatologically warmer regions towards Greenland (changes along horizontal axis) and diabatic processes (changes along vertical axis). For a more detailed discussion of this type of diagrams we refer to Papritz (2020).

The commonalities of all climatological air masses arriving over the GrIS include diabatic (radiative) cooling, as well as weak subsidence on the order of 25-50 hPa with associated adiabatic warming during the 8–2 d prior to arrival on the GrIS. This leads to a nearly isothermal temperature evolution in this period (Fig. 12a). Subsidence and poleward motion are both associated with transport from potentially warmer to a colder regions. Since this transport occurs at a rate exceeding that of diabatic cooling, the trajectories acquire a weak potential temperature anomaly of +1–2 K until two days before arrival on the GrIS (Fig. 12b). Within the last one to two days, air masses ascend nearly adiabatically to the GrIS and those arriving in region E additionally descend during the final 12 h (Fig. 12a). During this final period, the potential temperature anomaly fades away and the climatological air mass arrives on the diagonal in the $\theta - \theta_{cl}$ space (Fig. 12b).

Now considering melt air masses, we see that they are initially around 5 K (E) to 18 K (C) warmer and evolve in a distinct way from the climatological summertime air masses (compare Figs. 12a, c). The differences are most striking for C air masses. During the first four days, these air masses remain at around 800 hPa (Fig. 12c) with no substantial local potential temperature anomaly (Fig. 12d). Then, within two to three days, they experience diabatic heating of around 6 K while ascending by nearly 250 hPa (Fig. 12c) and a potential temperature anomaly of more than 7 K forms (Fig. 12d). Note that the formation of the potential temperature anomaly is about equally due to diabatic heating and transport into a climatologically colder region at the beginning and end of the backward trajectories. Overall, C melt air masses experience a strong cooling of 15 K in eight days, while their potential temperature slightly increases.

In contrast, E, N, and S air masses have an evolution in $\theta - T$ space that is more similar to climatological air masses (Fig. 12c). Notable differences include reduced diabatic cooling and larger ascent and an associated decrease of temperature during the final two to three days, which is consistent with an origin at lower altitudes. Furthermore, the descent of air masses arriving in region E is more pronounced. The decisive difference between melt event air masses and their climatological reference is, therefore, the much higher T and θ values at $t = -192$ h. E, N, and S air masses show a similar evolution in $\theta - \theta_{cl}$ space as climatological air parcels, but with a stronger effect of transport that results in final potential temperature anomalies of about +3–5 K (Fig. 12d). The gradual increase of the potential temperature anomalies along with the similar temporal evolution as climatological air masses highlights the importance of the anomalous origin and the enhanced poleward transport for the anomalous nature of melt event air masses.

In summary, we note that air masses associated with melt over the GrIS accumulation zone have no initial potential temperature anomaly but they originate from climatologically warmer regions further to the South. The atmospheric circulation, characterized by a large positive geopotential anomaly over Southeast Greenland, then induces strong poleward transport

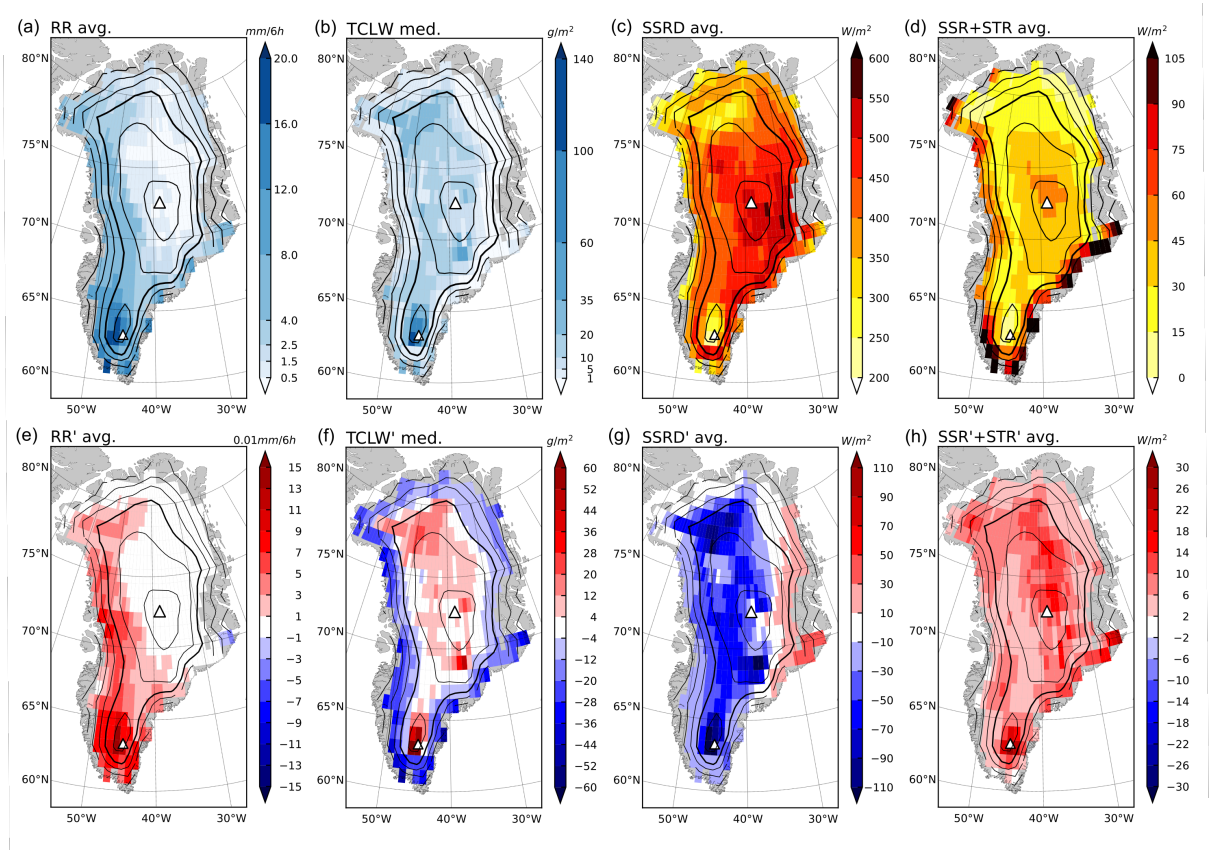

Figure 13. As Fig. 7 but for melt trajectories during all ~~Greenland~~ large-scale melt events.

towards the western GrIS, ascent, and latent heat release. Combined with the warmer origin of air masses, these diabatic temperature modifications are altogether responsible for the anomalously warm nature of the air masses when arriving over the GrIS. The importance of diabatic temperature modifications depends strongly on the altitude of the trajectory arrival position and are most important for air masses arriving near Summit.

4.3 Linkage to clouds and radiative effects

As in Section 3.3 for EV69, we analyze here the distribution of rainfall, total cloud liquid water, and surface radiation from ERA-Interim at 1° horizontal resolution, i.e., being most meaningful over the GrIS accumulation zone (Fig. 13)~~, which are key quantities modulating the surface energy balance during the 77 observed melt events~~. As for EV69, there is a clear distinction between the regions west of the ice divide (including large parts of regions C, N, and S), which are exposed to the moist-warm anticyclonic inflow, and the eastern GrIS, which is located on the lee side of the of the ice divide and thus is affected to a much smaller degree by the increased total column horizontal water vapour transport (Fig. 9).

On average, more rain falls in regions NW, S, and W (Figs. 13a, e), especially around Southdome, where a strong shift of precipitation from snow to rain occurs (not shown). Everywhere except region E, there is less incoming solar radiation during melt events compared to climatology (Fig. 13g). In fact, in ~~the higher elevated regions~~ regions above 2000 m this roots in a shift towards higher *TCLW*, i.e., a phase shift to the liquid regime and potentially also more cloud cover (Fig. 13f). Even though *TCLW* is reduced at ~~lower elevations~~ elevations below 2000 m along region W, there is sufficient cloud cover to reduce the incoming shortwave radiation. In contrast, in region E, related to descending air masses, little rain and reduced *TCLW* are a sign of clear-sky conditions, enabling *SSRD* to be very close to its maximum for this latitude and time of the year (Figs. 13a, f, g). Furthermore, the median total column water vapour anomaly is positive over the entire GrIS with an area-weighted average of $+2.8\,\mathrm{kg\,m^{-2}}$ (Fig. ~~S3f~~S4f). Despite the reduction of shortwave radiation west of the divide of the GrIS, the sum of net surface short- and longwave radiation is increased everywhere on the GrIS with an area-weighted average of $+7.3\,\mathrm{W\,m^{-2}}$ ($+2.1\,\mathrm{cm\,day^{-1}}$ melting potential calculated as in Sect. 3.3; Fig. 13h).

~~In light of the disputed sign of the cloud radiative effect over the GrIS~~To summarize, we find ~~that the warm-moist conditions during melt events as such increase the sum of incident short- and longwave radiation~~ an increase of net surface radiation during large-scale melt events, even though long- and shortwave contributions vary regionally~~as described above. The~~. The ERA-Interim-derived results are, however, representative for the bright GrIS accumulation zone only. The warm-moist anticyclonic flow conditions relate to an increase of downward longwave radiation ~~is on average increased by~~ by on average $+35.6\,\mathrm{W\,m^{-2}}$ ~~and even more at high elevations~~. In the upper accumulation zone, where the cloud water phase ~~shifts, peaking at Southdome with an anomaly of~~ is shifted wrt. climatology, this anomaly peaks at $+99.6\,\mathrm{W\,m^{-2}}$ near Southdome (Fig. ~~S3h~~S4h). ~~The results here confirm~~ Our findings underline the importance of ~~moisture transport by the prevailing anticyclonic weather regime for Greenland melt events~~ longwave radiative forcing - initially induced by meridional moisture transport - for melt events affecting large parts of the GrIS accumulation zone (Fig. 9)~~via the longwave radiative effects of water vapour and clouds~~, as previously highlighted by Mattingly et al. (2016), Van Tricht et al. (2016), ~~Ding et al. (2017) and Hofer et al. (2019). We conclude that during melt events:~~

1. ~~moistening of the atmospheric column increases the incoming longwave radiation over the entire GrIS;~~
2. ~~liquid clouds that were most prominent regions S, NW, and W go along with less incident shortwave radiation and thus reduce melt especially in the ablation area by preventing the strong shortwave ice albedo feedback (Box et al., 2012; Wang et al., 2019 but are highly dependent on the interplay of albedo and optical cloud properties (Van den Broeke et al., 2008);~~
3. ~~rain, mostly affecting the same regions as (2), enhances melt (i) directly by its positive temperature, (ii) indirectly through the albedo feedback by darkening the surface (Fausto et al., 2016), and (iii) by thereby precondition the ice surface for following melt;~~
4. ~~clouds in the high albedo accumulation region C have a net warming effect at the surface, especially with the observed higher liquid water content and if their optical thickness lies in the optimal intermediate range as during EV69 (Bennartz et al., 2013; S~~

~~Thus, our results indicate that during melt events, the synoptic circulation and transport patterns favour a distribution of cloud (and moisture) radiative effects that potentially enhance melt all over the GrIS because processes (1), (3), and (4) overcompensate the competing shortwave cooling effect (2).~~ Wang et al. (2019), Hofer et al. (2019), and Izeboud et al. (2020).

5 Discussion and Conclusions

5.1 Large-scale Greenland melt events

We found 77 large-scale Greenland melt events during JJA 1979–2017 of more than one day duration (Question Q1, Sect. 1) by identifying melt of the Greenland Ice Sheet (GrIS) with a skin temperature $\geq -1°C$ from ERA-Interim data together with an elevation- and extent-based selection criterion (Sect. 2.2). These events became 60% more frequent and on average about two days longer between the reference periods "recent past" (1986–2005) and "present day" (2005–2015) of the IPCC Special Report on the Ocean and Cryosphere in a Changing Climate (SROCC; Mintenbeck et al., 2020). Melt events longer than ten days, unprecedented in the "recent past", accounted for 18% of the "present day" melt events. Obviously, these trends follow from global warming (Johannessen et al., 2004), characterized by a pronounced warming in the Arctic ~~known as Arctic amplification (e.g., Serreze and Barry, 2011)~~(e.g., Serreze and Barry, 2011), and large-scale melt events are expected to cover the entire ice sheet in the near future (Box et al., 2012). However, it is interesting to briefly discuss the importance of climate warming as compared to circulation-induced warming for the occurrence and spatial extent of melt events.

The JJA near-surface potential temperature (θ_{10m}) correlates well ($r = 0.66$) with the cumulative melt extent (CME) obtained from accumulating melt extent over all melt event time steps (see Section 2.2) in a given summer (Fig. 14a). This is especially noteworthy considering the asymmetry of the CME timeseries, which only varies in the presence of melt events but not when they are absent (i.e., CME ≥ 0). Despite the higher correlation of CME with climate warming ($r = 0.57$; Fig. 14b), there is a clear relationship between the seasonal circulation-induced θ_{10m} anomaly and CME ($r = 0.41$; Fig. 14c). Circulation can amplify warming by a factor of two, e.g., in summers 2010 and 2012, which belonged to the series of summers with persistent NAO-/GBI+ summer circulation anomalies (Fettweis et al., 2013; Hanna et al., 2018). Likewise, circulation can also offset climate warming such as in summers 2009 and 2015. The exceptional melt event EV69, discussed here as a case study, was part of - and contributing to - the warmest summer on record (2012; $\theta'_{10m} = +2.6 \pm 0.6$ K). EV69 is a textbook example of a ~~Greenland~~ large-scale melt event as most of the general dynamical and thermodynamic characteristics of melt events were strongly pronounced.

5.2 Large-scale air mass transport and transformations contributing to melt events

The most prominent synoptic characteristic of ~~Greenland~~ large-scale melt events is a upper-level ridge or tropospheric cut-off with its center located southeast of Greenland (Q2, Sect. 1). Despite the anomalously strong final descent of air masses arriving

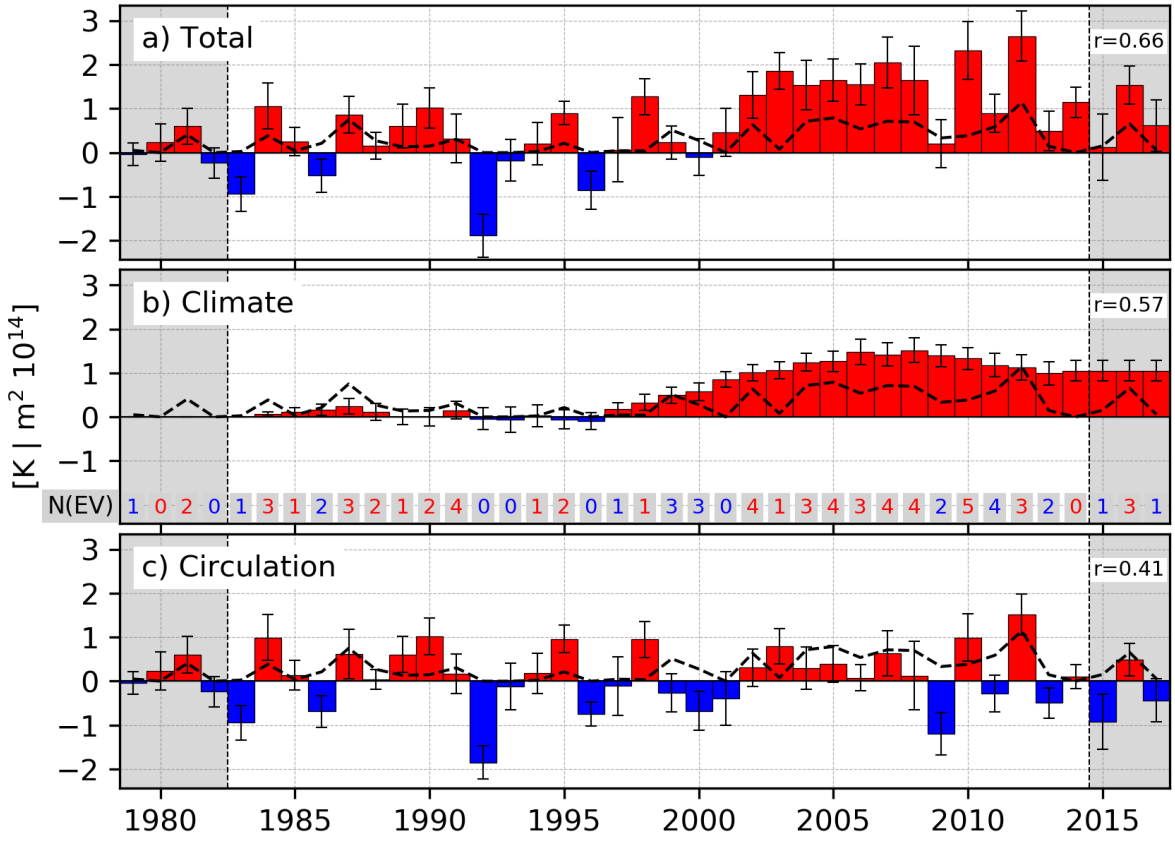

Figure 14. A time series of the (a) total, (b) climatological (9-yr centered running mean), and (c) circulation-induced (i.e., total minus climatological) near-surface potential temperature anomaly, $\theta'_{10\mathrm{m}}$, temporally averaged over JJA and spatially (standard deviation shown by whiskers) over the GrIS. The time series are shown wrt. the climatology at the beginning of the time series (1979/1983), and their correlation with the cumulative melt extent during melt events (dashed line) is given in the upper right of each panel. Numbers in (b) indicate the number of ~~Greenland~~ large-scale melt events in this summer, colored according to (c). Due to the running mean used in (b), the decomposition of the temperature anomaly shown in (b) and (c) is only meaningful in the period 1983–2014.

in central and eastern Greenland during these events, large-scale subsidence and adiabatic warming within the anticyclonic flow anomaly is of very little importance for ~~Greenland~~ the identified melt events. This is opposed to lower tropospheric warm extremes in the central Arctic (Binder et al., 2017; Papritz, 2020) and in mid-latitude heat waves (Bieli et al., 2015; Zschenderlein et al., 2019). The location of the geopotential height anomaly southeast of Greenland is favourable for inducing a southerly flow and enhanced total column horizontal water vapour transport to the West and towards the southern tip of Greenland. As these air masses impinge on Greenland's orography, they are forced to ascend, accompanied by cloud formation and precipitation, subsequently followed by anticyclonic transport across the GrIS and eventually descent along the eastern slope of the ice

sheet.

The two most important processes contributing to the warm anomaly of air masses of ~~Greenland~~ large-scale melt events are (Q3, Sect. 1):

1. **Transport:** Melt event air masses originate from a region that is 15 K warmer than climatological air masses. ~~At~~ However, at their origin eight days prior to arrival in Greenland, melt event air masses are ~~, however,~~ not generally anomalously warm. Hence, it is their origin at lower latitude and/or lower altitude and the subsequent rapid meridional transport of up to 40° latitude that are decisive for their final temperature anomaly. During transport to the GrIS accumulation zone, the melt air masses cool more than usual, i.e., by ∼15 K, which keeps ~~the trajectories~~ those arriving closest to the surface just above the critical threshold to induce melt. As we found, the warm anomaly associated with air masses that arrived near Summit during EV69 arose due to strong meridional transport to Greenland and did not result from a pre-existing warm anomaly such as associated with a heat wave in the Great Plains of North America (Hoerling et al., 2014; Neff et al., 2014; Bonne et al., 2015).

2. **Latent heat release:** As the GrIS has an average elevation of more than 2000 m, airstreams ascend either dynamically or orographically along their 8-day trajectory. This ascent occurs at the poleward edge of a band of prominent horizontal moisture transport. Latent heat release during ascent and, consequently, cloud formation is contributing substantially to the final warm anomaly of air masses arriving over the ~~plateau region~~accumulation zone. Both processes, meridional transport and latent heating, are most pronounced for the ~~high-elevation, central regions of the GrIS. Air masses causing melt higher on the GrIS come from~~ upper accumulation zone, i.e., the central GrIS. The higher in the GrIS accumulation zone air masses arrive, the warmer and more southerly ~~regions and experience~~ is their region of origin, and the more the experienced diabatic warming and adiabatic cooling ~~that deviates more~~ deviates from the climatological summertime air parcel (Q4, Sect. 1). Melt air masses of the northern and southern GrIS undergo ascent later along their 8-day trajectory and have an origin at lower levels than air masses of the central GrIS.

~~We further find that the melt events go along with increased~~

5.3 Air mass impact on the GrIS

We specifically investigated the air mass history and the related near-surface conditions during large-scale melt events, which affect large parts of the GrIS accumulation zone (Sect. 2.2). During such events, total column water vapour ~~(everywhere), related to the~~ is increased, associated with an enhanced poleward moisture transport ~~, and~~ and with a phase change of cloud water and precipitation from ice to liquid~~forming~~. The latter forms where airstreams ascend over the southern tip of Greenland, along the west coast, as well as in the North of the GrIS (Q3, Sect. 1). ~~The resulting net radiative anomaly contributes positively~~ Therefore, the incident shortwave radiation is reduced over the western and central GrIS, while the opposite applies for the clear-sky regions east of the ice divide. The net surface radiation anomaly is positively contributing to surface melt ~~during Greenland melt events (GrIS-wide area-weighted average melting potential of 2.1 cm ice day^{-1}), especially in high-elevated~~

regions and the Northwest of the GrIS. Clear-sky conditions prevail over the eastern GrIS , resulting in reduced total column water and enhanced incoming over the entire GrIS accumulation zone, and is only in the very East dominated by shortwave radiation. In contrast, the enhanced liquid water content in the elevated regions in the South, West and North of the GrIS lead to a reduction of incident shortwave radiation. Yet, the net radiation anomaly is positive due to enhanced longwave radiation. Generally, downward longwave radiation accumulation zone causes an anomalously strong longwave radiative forcing, relating to the net cloud warming observed in these regions (Wang et al., 2019). This is a key element in triggering process for surface melt in Greenland the GrIS accumulation zone and the remaining Arctic (Mortin et al., 2016; Lee et al., 2017), and enhanced poleward moisture transport improves the simulation of Arctic clouds and near-surface temperature (Baek et al., 2020). The dynamical and thermodynamic characteristics of melt event air masses found here, confirm the importance of poleward moisture transport as a result of the long-range transport of air masses from the South towards Greenland for (i) inducing latent heating along the trajectory, and (ii) causing a positive cloud radiative effect over the GrIS accumulation zone.

Over the low albedo ablation zone, where the majority of GrIS surface mass loss occurs, the cloud radiative effect is typically cooling as shortwave radiation drives surface melt via the more efficient albedo-melt feedback (Hofer et al., 2017; Izeboud et al., 2020). While ERA-Interim is able to reproduce the warming cloud radiative effect over the accumulation zone during summer (Wang et al., 2019), the ablation zone is insufficiently represented in our data set and, therefore, precluded from the analysis. First and foremost, an accurate representation of the low ablation area albedo in summer ($0.3 - 0.5$) would be crucial to determine the surface melt resulting from the synoptic forcing during melt events (Izeboud et al., 2020). Also, the steep topography of the $20 - 100$ km wide ablation zone is not resolved in ERA-Interim (~ 100 km grid spacing). There, the impact of the presented melt air masses could in future work be studied with regional climate models such as MAR (Fettweis et al., 2017), or RACMO (Noël et al., 2016), which are run on the kilometer-scale including more sophisticated surface schemes. Also, the latest generation of reanalysis data, ERA5, with 0.5° horizontal resolution improves the simulated near-surface climate over Greenland to some degree (Delhasse et al., 2020).

As the large-scale

5.4 Importance of upper-tropospheric ridges

As the atmospheric dynamics is found to be the key driver of Greenland large-scale melt events, the understanding of upper-tropospheric ridges and blocks and their development and lifespan is highly relevant to Greenland's climate, GrIS mass loss (Hanna et al., 2014; Van den Broeke et al., 2017), and global sea-level rise (Van den Broeke et al., 2016; Box et al., 2018). The dynamical understanding of blocks (Pfahl et al., 2015; Steinfeld and Pfahl, 2019) and heat extreme-related upper-tropospheric ridges (Zschenderlein et al., 2020) now includes the important role of upstream latent heating for establishing and maintaining the negative potential vorticity anomalies in the upper troposphere. The representation of those processes in climate models is yet uncertain. More generally, global climate models are yet not able to capture the strong and persistent NAO- circulation anomalies of recent years (Fettweis et al., 2012, 2013). If these changes are the result of natural variability, long-term trends predicted by the models could still be trustworthy, as the model performance may mainly be limited by the internal variability

of the climate system (Fischer et al., 2013; Knutti and Sedláček, 2013). In the long run, Greenland blocking is not predicted to change significantly towards the end of this century (e.g., Gillett and Fyfe, 2013). If, however, the current decrease in summer NAO is a manifestation of systematic circulation changes associated with global warming, the ability of today's climate models to simulate future trends in the North Atlantic circulation is questionable, and GrIS mass loss at the end of this century could be underestimated by a factor of two (Delhasse et al., 2018). Given the importance of upper-tropospheric ridges and blocks, and associated transport of moist-warm air for ~~Greenland~~ large-scale melt events, future work should, therefore, focus on their representation, life-cycle and trends in climate models.

Code and data availability. All results are based on ERA-Interim data, which can be downloaded from ECMWF (https://apps.ecmwf.int/datasets/data/interim-full-daily/levtype=sfc/), and analyzed with two additional tools: LAGRANTO (Wernli and Davies, 1997; Sprenger and Wernli, 2015) and clim-ei (Sprenger et al., 2017). Scripts used for the analyses and plotting, mostly written in Python 3.7, are available on request from the authors.

Author contributions. MH performed most of the analyses, supported by LP, and wrote a first version of the manuscript based on his MSc thesis (Hermann, 2019). All authors contributed to the design of the study, the interpretation of the results and the writing.

Competing interests. The authors declare that they have no conflict of interest.

Acknowledgements. We thank the reviewers for their constructive feedback on the first version of the manuscript. We acknowledge the ECMWF for providing access to ERA-Interim data, and Michael Sprenger (ETH Zurich) for technical support with the LAGRANTO and clim-ei tool. This study has been partially funded by the H2020 European Research Council (INTEXseas; grant no. 787652).

References

Andersen, M. L., Stenseng, L., Skourup, H., Colgan, W., Khan, S. A., Kristensen, S. S., Andersen, S. B., Box, J. E., Ahlstrøm, A. P., Fettweis, X., and Forsberg, R.: Basin-scale partitioning of Greenland ice sheet mass balance components (2007–2011), Earth Planet. Sci. Lett., 409, 89–95, https://doi.org/10.1016/j.epsl.2014.10.015, 2015.

Baek, E.-H., Kim, J.-H., Park, S., Kim, B.-M., and Jeong, J.-H.: Impact of poleward heat and moisture transports on Arctic clouds and climate simulation, Atmospheric Chemistry and Physics, 20, 2953–2966, https://doi.org/10.5194/acp-20-2953-2020, 2020.

Bennartz, R., Shupe, M. D., Turner, D. D., Walden, V. P., Steffen, K., Cox, C. J., Kulie, M. S., Miller, N., and Pettersen, C.: July 2012 Greenland melt extent enhanced by low-level liquid clouds, Nature, 496, 83–86, https://doi.org/10.1038/nature12002, 2013.

Bieli, M., Pfahl, S., and Wernli, H.: A Lagrangian investigation of hot and cold temperature extremes in Europe, Quart. J. Roy. Meteor. Soc., 141, 98–108, https://doi.org/10.1002/qj.2339, 2015.

Binder, H., Boettcher, M., Grams, C. M., Joos, H., Pfahl, S., and Wernli, H.: Exceptional air mass transport and dynamical drivers of an extreme wintertime Arctic warm event, Geophys. Res. Lett., 44, 12 028–12 036, https://doi.org/10.1002/2017GL075841, 2017.

Bonne, J.-L., Steen-Larsen, H. C., Risi, C., Werner, M., Sodemann, H., Lacour, J.-L., Fettweis, X., Cesana, G., Delmotte, M., Cattani, O., Vallelonga, P., Kjær, H. A., Clerbaux, C., Sveinbjörnsdóttir, A. E., and Masson-Delmotte, V.: The summer 2012 Greenland heat wave: In situ and remote sensing observations of water vapor isotopic composition during an atmospheric river event, J. Geophys. Res. Atmos., 120, 2970–2989, https://doi.org/10.1002/2014JD022602, 2015.

Box, J. E., Bromwich, D. H., and Bai, L.-S.: Greenland ice sheet surface mass balance 1991–2000: Application of Polar MM5 mesoscale model and in situ data, J. Geophys. Res. Atmos., 109, D16 105, https://doi.org/10.1029/2003JD004451, 2004.

Box, J. E., Fettweis, X., Stroeve, J. C., Tedesco, M., Hall, D. K., and Steffen, K.: Greenland ice sheet albedo feedback: thermodynamics and atmospheric drivers, Cryosphere, 6, 821–839, https://doi.org/10.5194/tc-6-821-2012, 2012.

Box, J. E., Colgan, W. T., Wouters, B., Burgess, D. O., O'Neel, S., Thomson, L. I., and Mernild, S. H.: Global sea-level contribution from Arctic land ice: 1971–2017, Environ. Res. Lett., 13, 125 012, https://doi.org/10.1088/1748-9326/aaf2ed, 2018.

Cavallo, S. M. and Hakim, G. J.: Physical mechanisms of tropopause polar vortex intensity change, J. Atmos. Sci., 70, 3359–3373, https://doi.org/10.1175/JAS-D-13-088.1, 2013.

Chen, L., Fettweis, X., Knudsen, E. M., and Johannessen, O. M.: Impact of cyclonic and anticyclonic activity on Greenland ice sheet surface mass balance variation during 1980–2013, Int. J. Climatol., 36, 3423–3433, https://doi.org/10.1002/joc.4565, 2016.

Dee, D. P., Uppala, S. M., Simmons, A. J., Berrisford, P., Poli, P., Kobayashi, S., Andrae, U., Balmaseda, M. A., Balsamo, G., Bauer, P., Bechtold, P., Beljaars, A. C. M., van de Berg, L., Bidlot, J., Bormann, N., Delsol, C., Dragani, R., Fuentes, M., Geer, A. J., L, H., Healy, S. B., Hersbach, H., Hólm, E. V., Isaksen, L., Kållberg, P., Köhler, M., Matricardi, M., McNally, A. P., Monge-Sanz, B. M., Morcrette, J.-J., Park, B.-K., Peubey, C., de Rosnay, P., Tavolato, C., Thépaut, J.-N., and Vitart, F.: The ERA-Interim reanalysis: Configuration and performance of the data assimilation system, Quart. J. Roy. Meteor. Soc., 137, 553–597, https://doi.org/10.1002/qj.828, 2011.

Delhasse, A., Fettweis, X., Kittel, C., Amory, C., and Agosta, C.: Brief communication: Impact of the recent atmospheric circulation change in summer on the future surface mass balance of the Greenland ice sheet, Cryosphere, 12, 3409—3418, https://doi.org/10.5194/tc-12-3409-2018, 2018.

Delhasse, A., Kittel, C., Amory, C., Hofer, S., van As, D., S. Fausto, R., and Fettweis, X.: Brief communication: Evaluation of the near-surface climate in ERA5 over the Greenland Ice Sheet, Cryosphere, 14, 957–965, https://doi.org/10.5194/tc-14-957-2020, 2020.

Ding, Q., Schweiger, A., L'Heureux, M., Battisti, D. S., Po-Chedley, S., Johnson, N. C., Blanchard-Wrigglesworth, E., Harnos, K., Zhang, Q., Eastman, R., and Steig, E. J.: Influence of high-latitude atmospheric circulation changes on summertime Arctic sea ice, Nat. Clim. Change, 7, 289—295, https://doi.org/10.1038/nclimate3241, 2017.

Doyle, S. H., Hubbard, A., van de Wal, R. S. W., Box, J. E., van As, D., Scharrer, K., Meierbachtol, T. W., Smeets, P. C. J. P., Harper, J. T., Johansson, E., Mottram, R. H., Mikkelsen, A. B., Wilhelms, F., Patton, H., Christoffersen, P., and Hubbard, B.: Amplified melt and flow of the Greenland ice sheet driven by late-summer cyclonic rainfall, Nat. Geosci., 8, 647–653, https://doi.org/10.1038/ngeo2482, 2015.

Enderlin, E. M., Howat, I. M., Jeong, S., Noh, M.-J., Van Angelen, J. H., and Van Den Broeke, M. R.: An improved mass budget for the Greenland ice sheet, Geophys. Res. Lett., 41, 866–872, https://doi.org/10.1002/2013GL059010, 2014.

Fausto, R. S., van As, D., Box, J. E., Colgan, W., Langen, P. L., and Mottram, R. H.: The implication of nonradiative energy fluxes dominating Greenland ice sheet exceptional ablation area surface melt in 2012, Geophys. Res. Lett., 43, 2649–2658, https://doi.org/10.1002/2016GL067720, 2016.

Fettweis, X., Franco, B., Tedesco, M., Van Angelen, J. H., Lenaerts, J. T. M., Van den Broeke, M. R., and Gallée, H.: Estimating Greenland ice sheet surface mass balance contribution to future sea level rise using the regional atmospheric climate model MAR, Cryosphere, 6, 3101–3147, https://doi.org/10.5194/tc-7-469-2013, 2012.

Fettweis, X., Hanna, E., Lang, C., Belleflamme, A., Erpicum, M., and Gallée, H.: Important role of the mid-tropospheric atmospheric circulation in the recent surface melt increase over the Greenland ice sheet, Cryosphere, 7, 241–248, https://doi.org/10.5194/tc-7-241-2013, 2013.

Fettweis, X., Box, J. E., Agosta, C., Amory, C., Kittel, C., Lang, C., van As, D., Machguth, H., and Gallée, H.: Reconstructions of the 1900–2015 Greenland ice sheet surface mass balance using the regional climate MAR model, The Cryosphere, 11, 1015–1033, https://doi.org/10.5194/tc-11-1015-2017, 2017.

Fischer, E. M., Beyerle, U., and Knutti, R.: Robust spatially aggregated projections of climate extremes, Nat. Clim. Change, 3, 1033—1038, https://doi.org/10.1038/nclimate2051, 2013.

Gallagher, M. R., Shupe, M. D., and Miller, N. B.: Impact of atmospheric circulation on temperature, clouds, and radiation at Summit Station, Greenland, with self-organizing maps, J. Climate, 31, 8895–8915, https://doi.org/10.1175/JCLI-D-17-0893.1, 2018.

Gillett, N. P. and Fyfe, J. C.: Annular mode changes in the CMIP5 simulations, Geophys. Res. Lett., 40, 1189–1193, https://doi.org/10.1002/grl.50249, 2013.

Grams, C. M., Beerli, R., Pfenninger, S., Staffell, I., and Wernli, H.: Balancing Europe's wind-power output through spatial deployment informed by weather regimes, Nat. Clim. Chang., 7, 557—562, https://doi.org/10.1038/nclimate3338, 2017.

Hanna, E., Huybrechts, P., Janssens, I., Cappelen, J., Steffen, K., and Stephens, A.: Runoff and mass balance of the Greenland ice sheet: 1958-–2003, J. Geophys. Res. Atmos., 110, D13 108, https://doi.org/10.1029/2004JD005641, 2005.

Hanna, E., Jones, J. M., Cappelen, J., Mernild, S. H., Wood, L., Steffen, K., and Huybrechts, P.: The influence of North Atlantic atmospheric and oceanic forcing effects on 1900–2010 Greenland summer climate and ice melt/runoff, Int. J. Climatol., 33, 862–880, https://doi.org/10.1002/joc.3475, 2013.

Hanna, E., Fettweis, X., Mernild, S. H., Cappelen, J., Ribergaard, M. H., Shuman, C. A., Steffen, K., Wood, L., and Mote, T. L.: Atmospheric and oceanic climate forcing of the exceptional Greenland ice sheet surface melt in summer 2012, Int. J. Climatol., 34, 1022–1037, https://doi.org/10.1002/joc.3743, 2014.

Hanna, E., Hall, R. J., Cropper, T. E., Ballinger, T. J., Wake, L., Mote, T., and Cappelen, J.: Greenland blocking index daily series 1851—2015: analysis of changes in extremes and links with North Atlantic and UK climate variability and change, Int. J. Climatol., 38, 3546–3564, https://doi.org/10.1002/joc.5516, 2018.

Heinemann, G. and Klein, T.: Modelling and observations of the katabatic flow dynamics over Greenland, Tellus A: Dynamic Meteorology and Oceanography, 54, 542–554, https://doi.org/10.3402/tellusa.v54i5.12167, 2002.

Hermann, M.: A Lagrangian analysis of the dynamical and thermodynamic drivers of Greenland warm events during 1979–2017, 2019.

Hoerling, M., Eischeid, J., Kumar, A., Leung, R., Mariotti, A., Mo, K., Schubert, S., and Seager, R.: Causes and predictability of the 2012 Great Plains drought, Bull. Amer. Meteor. Soc., 95, 269–282, https://doi.org/10.1175/BAMS-D-13-00055.1, 2014.

Hofer, S., Tedstone, A. J., Fettweis, X., and Bamber, J. L.: Decreasing cloud cover drives the recent mass loss on the Greenland ice sheet, Sci. Adv., 3, e1700 584, https://doi.org/10.1126/sciadv.1700584, 2017.

Hofer, S., Tedstone, A. J., Fettweis, X., and Bamber, J. L.: Cloud microphysics and circulation anomalies control differences in future Greenland melt, Nat. Clim. Chang., 9, 523–528, https://doi.org/10.1038/s41558-019-0507-8, 2019.

Holton, J. R. and Hakim, G. J.: An introduction to dynamic meteorology, vol. 88, Academic Press, 5th edn., 2012.

Hurrell, J. W., Kushnir, Y., Ottersen, G., and Visbeck, M.: An overview of the North Atlantic oscillation, pp. 1–35, American Geophysical Union (AGU), https://doi.org/10.1029/134GM01, 2013.

Izeboud, M., Lhermitte, S., Van Tricht, K., Lenaerts, J. T. M., Van Lipzig, N. P. M., and Wever, N.: The Spatiotemporal Variability of Cloud Radiative Effects on the Greenland Ice Sheet Surface Mass Balance, Geophys. Res. Lett., 47, e2020GL087 315, https://doi.org/10.1029/2020GL087315, 2020.

Johannessen, O. M., Bengtsson, L., Miles, M. W., Kuzmina, S. I., Semenov, V. A., Alekseev, G. V., Nagurnyi, A. P., Zakharov, V. F., Bobylev, L. P., Pettersson, L. H., Hasselmann, K., and Cattle, H. P.: Arctic climate change: observed and modelled temperature and sea-ice variability, Tellus A, 56, 328–341, https://doi.org/10.3402/tellusa.v56i4.14418, 2004.

Kjeldsen, K. K., Korsgaard, N. J., Bjørk, A. A., Khan, S. A., Box, J. E., Funder, S., Larsen, N. K., Bamber, J. L., Colgan, W., Van Den Broeke, M., Siggaard-Andersen, M.-L., Nuth, C., Schomacker, A., Andresen, C. S., Willerslev, E., and Kjær, K. H.: Spatial and temporal distribution of mass loss from the Greenland ice sheet since AD 1900, Nature, 528, 396—400, https://doi.org/10.1038/nature16183, 2015.

Knutti, R. and Sedláček, J.: Robustness and uncertainties in the new CMIP5 climate model projections, Nat. Clim. Change, 3, 369–373, https://doi.org/10.1038/nclimate1716, 2013.

Lee, S., Gong, T., Feldstein, S. B., Screen, J. A., and Simmonds, I.: Revisiting the Cause of the 1989–2009 Arctic Surface Warming Using the Surface Energy Budget: Downward Infrared Radiation Dominates the Surface Fluxes, Geophys. Res. Lett., 44, 10 654–10 661, https://doi.org/10.1002/2017GL075375, 2017.

Liniger, M. A. and Davies, H. C.: Substructure of a MAP streamer, Q. J. R. Meteorol. Soc., 129, 633–651, 2003.

Liu, C. and Barnes, E. A.: Extreme moisture transport into the Arctic linked to Rossby wave breaking, J. Geophys. Res. Atmos., 120, 3774–3788, https://doi.org/10.1002/2014JD022796, 2015.

Mattingly, K. S., Ramseyer, C. A., Rosen, J. J., Mote, T. L., and Muthyala, R.: Increasing water vapor transport to the Greenland ice sheet revealed using self-organizing maps, Geophys. Res. Lett., 43, 9250–9258, https://doi.org/10.1002/2016GL070424, 2016.

Miller, N. B., Shupe, M. D., Cox, C. J., Walden, V. P., Turner, D. D., and Steffen, K.: Cloud radiative forcing at Summit, Greenland, J. Clim., 28, 6267–6280, https://doi.org/10.1175/JCLI-D-15-0076.1, 2015.

Mintenbeck, K., Collins, M., Bindoff, N. L., and Poloczanska, E.: The IPCC special report on ocean and cryosphere in a changing climate–challenges, opportunities and future scenarios, in: Ocean Sciences Meeting 2020, AGU, 2020.

Mortin, J., Svensson, G., Graversen, R. G., Kapsch, M.-L., Stroeve, J. C., and Boisvert, L. N.: Melt onset over Arctic sea ice controlled by atmospheric moisture transport, Geophys. Res. Lett., 43, 6636–6642, https://doi.org/10.1002/2016GL069330, 2016.

Mouginot, J., Rignot, E., Bjørk, A. A., van den Broeke, M., Millan, R., Morlighem, M., Noël, B., Scheuchl, B., and Wood, M.: Forty-six years of Greenland ice sheet mass balance from 1972 to 2018, Proceedings of the National Academy of Sciences, 116, 9239—9244, https://doi.org/10.1073/pnas.1904242116, 2019.

Neff, W., Compo, G. P., Ralph, F. M., and Shupe, M. D.: Continental heat anomalies and the extreme melting of the Greenland ice surface in 2012 and 1889, J. Geophys. Res. Atmos., 119, 6520–6536, https://doi.org/10.1002/2014JD021470, 2014.

Nghiem, S. V., Hall, D. K., Mote, T. L., Tedesco, M., Albert, M. R., Keegan, K., Shuman, C., DiGirolamo, N. E., and Neumann, G.: The extreme melt across the Greenland ice sheet in 2012, Geophys. Res. Lett., 39, L20 502, https://doi.org/10.1029/2012GL053611, 2012.

Noël, B., Fettweis, X., Van De Berg, W. J., Van Den Broeke, M. R., and Erpicum, M.: Sensitivity of Greenland ice sheet surface mass balance to perturbations in sea surface temperature and sea ice cover: a study with the regional climate model MAR, Cryosphere, 8, 1871–1883, https://doi.org/10.5194/tc-8-1871-2014, 2014.

Noël, B., Jan Van De Berg, W., Machguth, H., Lhermitte, S., Howat, I., Fettweis, X., and Van Den Broeke, M. R.: A daily, 1 km resolution data set of downscaled Greenland ice sheet surface mass balance (1958-2015), Cryosphere, 10, 2361–2377, 2016.

Ohmura, A.: Physical basis for the temperature-based melt-index method, J. Appl. Meteorol. Climatol., 40, 753–761, https://doi.org/10.1175/1520-0450(2001)040, 2001.

Papritz, L.: Arctic lower tropospheric warm and cold extremes: horizontal and vertical transport, diabatic processes, and linkage to synoptic circulation features, J. Clim., 33, 993–1016, https://doi.org/10.1175/JCLI-D-19-0638.1, 2020.

Papritz, L. and Spengler, T.: A Lagrangian climatology of wintertime cold air outbreaks in the Irminger and Nordic Seas and their role in shaping air-sea heat fluxes, J. Climate, 30, 2717–2737, https://doi.org/10.1175/JCLI-D-16-0605.1, 2017.

Park, H.-S., Lee, S., Kosaka, Y., Son, S.-W., and Kim, S.-W.: The impact of Arctic winter infrared radiation on early summer sea ice, J. Climate, 28, 6281–6296, https://doi.org/10.1175/JCLI-D-14-00773.1, 2015.

Pfahl, S., Schwierz, C., Croci-Maspoli, M., Grams, C. M., and Wernli, H.: Importance of latent heat release in ascending air streams for atmospheric blocking, Nat. Geosci., 8, 610–614, https://doi.org/10.1038/ngeo2487, 2015.

Ridley, J. K., Huybrechts, P., Gregory, J. u., and Lowe, J.: Elimination of the Greenland ice sheet in a high CO2 climate, J. Clim., 18, 3409–3427, https://doi.org/10.1175/JCLI3482.1, 2005.

Serreze, M. C. and Barry, R. G.: Processes and impacts of Arctic amplification: A research synthesis, Glob. Planet. Change, 77, 85–96, https://doi.org/10.1016/j.gloplacha.2011.03.004, 2011.

Sodemann, H., Schwierz, C., and Wernli, H.: Interannual variability of Greenland winter precipitation sources: Lagrangian moisture diagnostic and North Atlantic oscillation influence, J. Geophys. Res. Atmos., 113, D03 107, https://doi.org/10.1029/2007JD008503, 2008.

Solomon, A., Shupe, M. D., and Miller, N. B.: Cloud–atmospheric boundary layer–surface interactions on the Greenland ice sheet during the July 2012 extreme melt event, J. Clim., 30, 3237–3252, https://doi.org/10.1175/JCLI-D-16-0071.1, 2017.

Sprenger, M. and Wernli, H.: The LAGRANTO Lagrangian analysis tool–version 2.0, Geosci. Model Dev., 8, 2569–2586, https://doi.org/10.5194/gmd-8-2569-2015, 2015.

Sprenger, M., Fragkoulidis, G., Binder, H., Croci-Maspoli, M., Graf, P., Grams, C. M., Knippertz, P., Madonna, E., Schemm, S., Škerlak, B., and Wernli, H.: Global climatologies of Eulerian and Lagrangian flow features based on ERA-Interim, Bull. Amer. Meteor. Soc., 98, 1739–1748, https://doi.org/10.1175/BAMS-D-15-00299.1, 2017.

Steinfeld, D. and Pfahl, S.: The role of latent heating in atmospheric blocking dynamics: a global climatology, Climate Dynamics, 53, 6159–6180, https://doi.org/10.1007/s00382-019-04919-6, 2019.

Stohl, A.: Characteristics of atmospheric transport into the Arctic troposphere, J. Geophys. Res. Atmos., 111, D11 306, https://doi.org/10.1029/2005JD006888, 2006.

Tedesco, M. and Fettweis, X.: Unprecedented atmospheric conditions (1948–2019) drive the 2019 exceptional melting season over the Greenland ice sheet, Cryosphere, 14, 1209–1223, https://doi.org/10.5194/tc-14-1209-2020, 2020.

Tedesco, M., Fettweis, X., Mote, T., Wahr, J., Alexander, P., Box, J., and Wouters, B.: Evidence and analysis of 2012 Greenland records from spaceborne observations, a regional climate model and reanalysis data, Cryosphere, 7, 615–630, https://doi.org/10.7916/D8J38SGV, 2013.

Van den Broeke, M., Smeets, P., Ettema, J., and Munneke, P. K.: Surface radiation balance in the ablation zone of the west Greenland ice sheet, J. Geophys. Res. Atmos., 113, D13 105, https://doi.org/10.1029/2007JD009283, 2008.

Van den Broeke, M., Box, J., Fettweis, X., Hanna, E., Noël, B., Tedesco, M., van As, D., van de Berg, W. J., and van Kampenhout, L.: Greenland ice sheet surface mass loss: Recent developments in observation and modeling, Curr. Clim. Change Rep., 3, 345–356, https://doi.org/10.1007/s40641-017-0084-8, 2017.

Van den Broeke, M. R., Enderlin, E. M., Howat, I. M., Kuipers Munneke, P., Noël, B. P., Jan Van De Berg, W., Van Meijgaard, E., and Wouters, B.: On the recent contribution of the Greenland ice sheet to sea level change, Cryosphere, 10, 1933–1946, https://doi.org/10.5194/tc-10-1933-2016, 2016.

Van Tricht, K., Lhermitte, S., Lenaerts, J. T. M., Gorodetskaya, I. V., L'Ecuyer, T. S., Noël, B., van den Broeke, M. R., Turner, D. D., and van Lipzig, N. P. M.: Clouds enhance Greenland ice sheet meltwater runoff, Nat. Comm., 7, 10 266, https://doi.org/10.1038/ncomms10266, 2016.

Wang, W., Zender, C. S., van As, D., and Miller, N. B.: Spatial distribution of melt season cloud radiative effects over Greenland: evaluating satellite observations, reanalyses, and model simulations against in situ measurements, J. Geophys. Res. Atmos., 124, 57–71, https://doi.org/10.1029/2018JD028919, 2019.

Wernli, H. and Davies, H. C.: A Lagrangian-based analysis of extratropical cyclones. I: the method and some applications, Quart. J. Roy. Meteor. Soc., 123, 467–489, https://doi.org/10.1002/qj.49712353811, 1997.

Wernli, H. and Papritz, L.: Role of polar anticyclones and mid-latitude cyclones for Arctic summertime sea-ice melting, Nat. Geosci., 11, 108–113, https://doi.org/10.1038/s41561-017-0041-0, 2018.

Wesslén, C., Tjernström, M., Bromwich, D. H., de Boer, G., Ekman, A. M. L., Bai, L.-S., and Wang, S.-H.: The Arctic summer atmosphere: an evaluation of reanalyses using ASCOS data, Atmospheric Chemistry and Physics, 14, 2605–2624, https://doi.org/10.5194/acp-14-2605-2014, 2014.

Woollings, T., Barriopedro, D., Methven, J., Son, S.-W., Martius, O., Harvey, B., Sillmann, J., Lupo, A. R., and Seneviratne, S.: Blocking and its response to climate change, Current Climate Change Reports, 4, 287–300, https://doi.org/10.1007/s40641-018-0108-z, 2018.

Zschenderlein, P., Fink, A. H., Pfahl, S., and Wernli, H.: Processes determining heat waves across different European climates, Q. J. R. Meteorol. Soc., 145, 2973–2989, https://doi.org/10.1002/qj.3599, 2019.

Zschenderlein, P., Pfahl, S., Wernli, H., and Fink, A. H.: A Lagrangian analysis of upper-tropospheric anticyclones associated with heat waves in Europe, Weather and Climate Dynamics Discussions, 2020, 1–26, https://doi.org/10.5194/wcd-2019-17, 2020.

Zwally, H. J., Giovinetto, M. B., Beckley, M. A., and Saba, J. L.: Antarctic and Greenland drainage systems, GSFC cryospheric sciences laboratory, available at icesat4.gsfc.nasa.gov/cryo_data/ant_grn_drainage_systems.php. Last accessed March, 1, 2015, 2012.